Verifying the Cosmological Utility of Type Ia Supernovae: Implications of a Dispersion in the Ultraviolet Spectra

R. S. Ellis[1], M. Sullivan[2,3], P. E. Nugent[4], D. A. Howell[2], A. Gal-Yam[1], P. Astier[5], D. Balam[6], C. Balland[5], S. Basa[7], R. G. Carlberg[2], A. Conley[2], D. Fouchez[8], J. Guy[5], D. Hardin[5], I. Hook[3], R. Pain[5], K. Perrett[2], C. J. Pritchet[6], N. Regnault[5]

rse@astro.caltech.edu

ABSTRACT

We analyze the mean rest-frame ultraviolet (UV) spectrum of Type Ia Supernovae (SNe) and its dispersion using high signal-to-noise Keck-I/LRIS-B spectroscopy for a sample of 36 events at intermediate redshift ($\overline{z}$=0.5) discovered by the Canada-France-Hawaii Telescope Supernova Legacy Survey (SNLS). We introduce a new method for removing host galaxy contamination in our spectra, exploiting the comprehensive photometric coverage of the SNLS SNe and their host galaxies, thereby providing the first quantitative view of the UV spectral properties of a large sample of distant SNe Ia. Although the mean SN Ia spectrum has not evolved significantly over the past 40% of cosmic history, precise evolutionary constraints are limited by the absence of a comparable sample of high quality local spectra. The mean UV spectrum of our $z \simeq$0.5 SNe Ia and its dispersion is tabulated for use in future applications. Within the high-redshift sample, we discover significant UV spectral variations and exclude dust extinction as the primary cause by examining trends with the optical SN color. Although

[1]California Institute of Technology, E. California Blvd, Pasadena CA 91125, USA

[2]Department of Physics and Astronomy, University of Toronto, 50 St. George Street, Toronto, ON M5S 3H4, Canada

[3]Department of Physics (Astrophysics), University of Oxford, Keble Road, Oxford OX1 3RH, UK

[4]Lawrence Berkeley National Laboratory, 1 Cyclotron Road, Berkeley, CA 94720, USA

[5]LPHNE, CNRS-IN2P3 and Universités Paris VI & VII, 4 Place Jussieu, 75252 Paris Cedex 05, France

[6]Department of Physics and Astronomy, University of Victoria, PO Box 2055 STN CSC, Victoria BC V8T1M8, Canada

[7]LAM, CNRS, BP8, Traverse du Siphon, 13376 Marseille Cedex 12, France

[8]CPPM, CNRS-IN2P3 and Université Aix-Marseille II, Case 907, 13288 Marseille Cedex 9, France

progenitor metallicity may drive some of these trends, the variations we see are much larger than predicted in recent models and do not follow expected patterns. An interesting new result is a variation seen in the wavelength of selected UV features with phase. We also demonstrate systematic differences in the SN Ia spectral features with SN lightcurve width in both the UV and the optical. We show that these intrinsic variations could represent a statistical limitation in the future use of high-redshift SNe Ia for precision cosmology. We conclude that further detailed studies are needed, both locally and at moderate redshift where the rest-frame UV can be studied precisely, in order that future missions can confidently be planned to fully exploit SNe Ia as cosmological probes.

Subject headings: surveys – supernovae: general – cosmological parameters

1. Introduction

Supernovae of Type Ia (SNe Ia) are now well-established as cosmological distance indicators. In addition to the original surveys by the Supernova Cosmology Project (SCP; Perlmutter et al. 1997, 1999) and the High-Z Supernova Search Team (Schmidt et al. 1998; Riess et al. 1998), a new generation of SN Ia surveys is underway both locally (Aldering et al. 2002; Li & Filippenko 2005; Hamuy et al. 2006) and at higher redshifts (Astier et al. 2006; Riess et al. 2007; Wood-Vasey et al. 2007). Despite the availability of independent probes of the presence and properties of dark energy from studies of the cosmic microwave background (Spergel et al. 2007) and galaxy redshift surveys (Efstathiou et al. 2002; Cole et al. 2005; Eisenstein et al. 2005), the luminosity distance–redshift relation for SNe Ia provides the only *direct* evidence for a cosmic acceleration.

The detection and characterization of dark energy, via measurements of the average cosmic equation of state parameter $<w>$, requires the precision measurement of SNe Ia to redshifts $z \simeq 0.5$–1, sampling the epoch of cosmic acceleration (Astier et al. 2006). However, more precise constraints on the nature of dark energy, for example evidence for any variation in w with redshift, requires extending these studies to redshift $z>1$ (Riess et al. 2004, 2007) where the early effects of deceleration may be detectable. As projects are developed which plan to probe SNe Ia beyond $z=1$ for this purpose (e.g Aldering 2005; Benford & Lauer 2006), it becomes important to understand the possible limitations of using SNe Ia as distance probes. Key issues relating to the diversity of SNe Ia and their possible evolution with redshift as a population, together with the limiting effects of dust and/or color corrections to their photometric properties, are particularly crucial to understand.

Several local studies (Hamuy et al. 1995; Riess et al. 1999; Hamuy et al. 2000; Howell 2001; Mannucci et al. 2005; Gallagher et al. 2005) have already indicated correlations between SN Ia properties and host galaxy morphologies. More recently, Sullivan et al. (2006b) have shown that the properties of distant SNe Ia appear to be a direct function of their local stellar population, with the distribution of light curve widths and hence peak luminosities correlating with the host galaxy specific star-formation rate. This work also determined that the rate of SNe Ia per unit stellar mass of their host galaxies is larger in actively star-forming galaxies, suggesting many must be produced quite rapidly in recently formed stellar populations, perhaps suggestive of more than one progenitor mechanism. The authors conclude that SNe Ia may well be a bimodal or a more complex population of events (see also Scannapieco & Bildsten 2005; Mannucci et al. 2006). Such diversity in the properties of SNe Ia could have far-reaching implications, particularly if the *mix* of mechanisms or delay times within the broad population gradually changes with look-back time (e.g. Mannucci et al. 2006; Sullivan et al. 2006b; Howell et al. 2007).

These recent developments, which illustrate how improved precision reveals new physical correlations in the SN Ia population, raise the broader question of whether future SN Ia experiments might be limited in precision by variations of a systematic nature within the population, for example with redshift, which cannot be removed via empirical correlations. Detailed local surveys such as the LOSS/KAIT (Li & Filippenko 2005) and CfA surveys (Riess et al. 1999; Jha et al. 2006) have presented valuable data on the homogeneity and trends in the SNe Ia population. Further promising work is being undertaken via the Supernova Factory (Aldering et al. 2002) and the Carnegie Supernova Project (Hamuy et al. 2006). Important though these continued programs will be, they are insufficient to address all possible concerns about the use of SNe Ia as precision tools in cosmology. Comparable studies at intermediate redshift[1] will be particularly important in order to address questions relating to possible evolutionary effects and environmental dependencies. In addition, it is not always practical at low redshift to cover the full wavelength range necessary to test for systematic trends.

In this paper we analyze high signal-to-noise ratio rest-frame ultraviolet (UV) spectra of a large sample of intermediate redshift SNe Ia drawn from the Canada-France-Hawaii Telescope Supernova Legacy Survey (SNLS; Astier et al. 2006), a rolling search which is particularly effective for locating and studying events prior to their maximum light. Our aim is obtain a substantially higher signal-to-noise in the spectra than that typically obtained during spectroscopic programs to type SNe and measure redshifts. We target the UV wave-

[1]Defined here to represent the range $0.2<z<0.7$.

length region because in this wavelength region the SN spectrum is thought to provide the most sensitive probe of *progenitor metallicity* (e.g. Höflich et al. 1998; Lentz et al. 2000), a variable which may shed light on the possibility of progenitor evolution. The time-dependent UV spectrum is also needed in estimating "cross-band" k-corrections, particularly at redshifts $z > 1$ where optical bandpasses probe the rest-frame near-UV (Riess et al. 2004, 2007). Little is known about the properties and homogeneity of the UV spectra of SNe Ia, largely because of the absence of suitable instruments for studying this wavelength range in local events. Although some local SN Ia UV spectra are available from International Ultraviolet Explorer (IUE) or Hubble Space Telescope (HST) satellite data (e.g. Leibundgut et al. 1991; Kirshner et al. 1993; Cappellaro et al. 1995), the bulk of the progress now possible in this area can be provided from optical studies of intermediate-redshift events with large ground-based telescopes.

The goals of this paper are thus to address the question of both the diversity and possible physical evolution in the intermediate redshift SN Ia family. We compare the rest-frame UV behavior of local SNe Ia with that derived for intermediate-redshift ($z \simeq 0.5$) events where the rest-frame UV enters the region of high efficiency of the Keck LRIS-B spectrograph. We also study the degree to which the UV spectra at intermediate redshift represent a homogeneous population, independent of other variables such as the physical environment and light curve stretch.

A plan of the paper follows. In § 2 we introduce the salient features of the SNLS and our method for selecting SNe Ia for detailed study. In § 3 we discuss the Keck spectroscopic observations and their reduction, including the treatment of host galaxy subtraction and flux calibration. In § 4 we consider our sample with respect to the broader set of SNe found by SNLS, ensuring it is a representative subset in terms of various observables, and discuss existing local UV spectra. In § 5, we undertake the detailed analysis. First we compare the UV spectra found in our sample with those found locally. We then examine the diversity of intermediate-redshift SNe Ia in various ways and correlate the UV variations with the light curves of the SNe and the properties of the host galaxies. We discuss these trends in terms of progenitor mechanisms in § 6 and examine the implications in terms of possible long term limitations of SNe Ia as probes of dark energy. We also present the mean phase-dependent SN Ia spectrum and its uncertainties for use in future work.

2. Selection of SNLS SNe Ia

Our SNe Ia are taken from the Supernova Legacy Survey (SNLS), a "rolling" search for distant SNe with a primary science goal of determining the average equation-of-state

parameter of dark energy, $<w>$ (see Astier et al. 2006). SNLS exploits the square-degree Megacam camera (Boulade et al. 2003) on the Canada-France-Hawaii Telescope (CFHT), and comprises repeat imaging in 4 filters, $g'r'i'z'$, of four deep 1×1 degree fields (see Sullivan et al. 2006a for the field coordinates), plus further $u^\star$ imaging which is not time-sequenced. Each field is imaged several (~ 5) times per lunation for 5-6 lunations per year. A description of the real-time search operations and the criteria for following SN candidates spectroscopically can be found in Sullivan et al. (2006a). Spectroscopic follow-up time for the essential work of basic redshift measurement and SN type determination for cosmological analyses comes from major long-term programs at the European Southern Observatory Very Large Telescopes (Basa et al., in prep; PI: Pain), the Keck observatory (PI: Perlmutter) and the Gemini North and South telescopes (Howell et al. 2005; Bronder et al. 2007, PI: Hook).

Observing time with the Keck-I telescope for the detailed spectroscopic study of individual SNe presented in this paper was scheduled from 2003 through 2005. The goal was to obtain substantially higher signal-to-noise ratio spectra than those required for SN typing (particularly in the rest-frame UV), and hence we targeted SNe Ia with a mean redshift lower than that of the SNLS as a whole ($\overline{z}$=0.45 versus $\overline{z}$=0.6) and used integration times $\sim$ 3–4 times longer for that redshift.

To avoid spectroscopic screening of every candidate (results from the mainstream VLT and Gemini programs were typically not available at the time of the Keck observations), a code was developed to constrain the redshift, SN type and epoch from the available photometric data (see Sullivan et al. 2006a, for details). In selecting candidates for this program, the following criteria were adopted:

1. The SN photometric redshift lay at z<0.75,
2. The predicted phase was such that the Keck observations would be conducted prior to or close to maximum light.
3. The light curve and color were consistent with a SN Ia,

In practise, this last criteria is conservatively applied to minimize the risk of selecting against SNe Ia which may differ from the template used in our selection code, though this reduces the fraction of SNe Ia observed: By the end of 2005, after 20 nights of Keck time, 58 SN candidates were observed of which 36 were confirmed as SNe Ia ($\sim$60%). A higher fraction of SNe Ia could have been obtained by a more rigorous application of the pre-selection technique; this argues that any bias introduced by our selection is small.

Table 1 summarizes the key parameters for the SNe Ia sampled in the Keck campaign (an independent survey of SNe IIP was also undertaken during this period (Nugent et al. 2006).)

We restrict these 36 SNe to a high-quality subset, removing 3 as spectroscopically peculiar (see § 5.1), 2 with a low-S/N Keck spectrum, and 5 with poor g' light curve coverage which precludes an accurate subtraction of the host galaxy from the SN spectrum (see Table 1). These later 5 were all observed during the SNLS "pre-survey" when the light curve coverage in g' was less dense, and hence our photometrically calibrated SN spectrum will suffer a greater systematic uncertainty (see § 3.3). Analysis of the remaining 26 SNe Ia forms the basis of this paper. Fig. 1 displays the redshift distribution of these high-quality SNe Ia and the breakdown in phase at which the Keck spectra were obtained.

For comparison purposes, we will also make use of an additional sample of 160 spectroscopically-confirmed SNLS SNe Ia (without high quality Keck coverage) within the above redshift range for which good broad-band photometric data is available. This will be used as a control to demonstrate our SN Ia selection is unbiased relative to the larger SNLS population in terms of fundamental properties such as light curve stretch, host galaxy type and location within each host.

3. Spectroscopic Data

3.1. Observations

All spectroscopic observations of SNLS SNe presented here were conducted with the 10 meter Keck-I telescope using the two-channel Low Resolution Imaging Spectrograph (LRIS; Oke et al. 1995). Although SNe Ia have broad absorption features, the need to monitor expansion velocities to reasonable precision as well as to locate narrower diagnostic lines which would otherwise be blended in broader features defined the need for intermediate (600 l mm^{-1}) dispersion gratings. Access to the rest-frame UV over $0.2<z<0.7$ was a prime goal given the sensitivity of features in this region to metallicity, temperature and photospheric expansion velocity.

Taking these considerations into account, we adopted a spectroscopic set up using a 400 line mm^{-1} grating blazed at 8500Å (giving a dispersion of $\simeq 1.9\,\text{Å}\,\mathrm{pix}^{-1}$) on the red side and a 600 line grism blazed at 4000Å (dispersion $\simeq 0.6\,\text{Å}\,\mathrm{pix}^{-1}$) on the blue side. With a 5600Å dichroic, this gave a contiguous wavelength coverage from the atmospheric limit on the blue side through to 9400Å on the red side. On some of the earliest runs in 2003, we experimented with a 300 line grism blazed at 5000Å (dispersion $\simeq 1.4\,\text{Å}\,\mathrm{pix}^{-1}$) on the blue side and a 600 line grating blazed at 7500Å (dispersion $\simeq 1.3\,\text{Å}\,\mathrm{pix}^{-1}$) on the red side with a 6800Å dichroic. This provided a lower resolution on the blue side, but a more optimal set up on the red side for the higher redshift SNe. However, we found the 6800Å dichroic did

not permit accurate flux calibration on the blue side, because of residual contamination in the second order of diffraction. In very good seeing conditions, we used a 0.7″ slit, otherwise a 1″ slit was used.

Observations were performed at the parallactic angle (e.g. Filippenko 1982). Each individual exposure was typically between 1200-1800s, and the SN was dithered along the slit by 3-5″ between exposures to aid with fringe removal in the data reduction. The telescope was refocused periodically during each night from which an estimate of the seeing was measured. Table 2 summarizes these spectroscopic observations.

3.2. Data Reduction

All spectroscopic data were processed using a pipeline developed by one of us (MS). This pipeline uses both standard Image Reduction and Analysis Facility (IRAF[2]) software as well as our own custom-written routines. LRIS is a two-arm spectrograph and different reduction techniques are required on each side as the red side suffers significant fringing above 7000Å.

Our first step is to remove the overscan level on each amplifier of each CCD, and then subtract a master zero-frame constructed on the afternoon of each night of observing to remove any bias pattern. Both sides are then divided by a normalized internal flat-field which removes pixel-to-pixel sensitivity variations. This division also corrects for the different gains of the LRIS CCD amplifiers. The 0.7″ slit additionally requires division by a "slit-flat" or "illumination" flat-field as the slit illumination is quite uneven, presumably due to milling defects in the slit. An additional complication is that the spatial position of the slit on the CCD can drift by several pixels over the course of the night, so the slit-flat is shifted to best match each observation. Cosmic-rays are then identified using LACOSMIC (van Dokkum 2001) and removed via interpolation from neighboring pixels.

We perform our sky subtraction following the technique of Kelson (2003), which subtracts a two-dimensional sky frame constructed from sub-pixel sampling of the background spectrum and a knowledge of the wavelength distortions as determined from two-dimensional arc comparison frames. For the blue side, we proceed directly to the spectral extraction after sky subtraction; on the red side we perform an additional fringe correction before extraction.

---

[2]IRAF is distributed by the National Optical Astronomy Observatories, which are operated by the Association of Universities for Research in Astronomy, Inc., under cooperative agreement with the National Science Foundation.

To generate the master fringe frame, we first divide every sky-subtracted frame by the two-dimensional sky frame that was subtracted and that caused the fringing, resulting in a two-dimensional map of the fringe strengths per photon for each exposure. All individual fringe maps taken in a given configuration are averaged with sigma-clipping to form a master fringe frame, masking out regions in each exposure that contain object flux, and weighting each frame by the exposure time of the observation. As the observations are dithered, the objects are located on a different part of the CCD in each frame, and the fringe strength at every pixel is therefore sampled across an entire night. Finally, we boxcar smooth the master fringe frame to increase the signal-to-noise ratio in the fringes, which typically extend over several pixels. This smoothed, master fringe frame is then scaled and subtracted from each red-side exposure at the stage prior to sky-subtraction, and the sky-subtraction then repeated on the fringe-subtracted images.

The two-dimensional frames are transformed to a constant dispersion using comparison arc lamp images. Because the objects under study typically have a reasonable signal-to-noise ratio, the spectral extraction was performed by tracing the object position on the CCD and using a variance-weighted extraction in a seeing matched aperture, equal to 1.25 times the seeing. An error spectrum from the statistics of the photon noise is also extracted at the same time. The wavelength calibration of each extracted spectrum is then tweaked using the position of the night-sky lines to account for any drift in the wavelength solution during a given night. We then perform an approximate telluric and relative flux calibration using spectrophotometric standard stars taken from Massey et al. (1988), and correcting for typical Mauna Kea atmospheric extinction using the extinction law of Krisciunas et al. (1987) and the effective airmass of each exposure. We note that flux calibration errors introduced during this process that vary smoothly as a function of wavelength will be corrected by our calibration to the SN lightcurves described in the next section.

Following optimal combination of the different exposures and relative flux calibration of the blue and red components, our final step is to scale the two sides into a single calibrated spectrum. We first match the flux across the dichroic by defining narrow box filters either side of the dichroic and scale each spectrum appropriately. We then use a weighted mean to combine the spectra, in the process re-binning to a constant 2Å per pixel resolution. The result is a contiguous science spectrum, together with an error spectrum representing the statistical uncertainties in the flux in each binned pixel.

Where possible, we measure redshifts from lines in the host galaxy spectrum. In some cases the host galaxy was too faint, or the SN too isolated from the host galaxy, to measure a redshift from the galaxy lines, and the redshift was determined from template fits to the SN spectrum (e.g. Howell et al. 2002). As a final step prior to scientific analysis we interpolate

across the positions of host galaxy emission features (e.g., Hα, Hβ, O II, etc.) to remove these from the spectra.

The SNe Ia themselves were identified by a lack of hydrogen in their spectra, combined with broad (several thousand $\mathrm{km\,s^{-1}}$) P Cygni lines of elements such as Si II, S II, Ca II, Mg II, and blends of Fe peak lines. The classification of SNe is discussed extensively in the literature; see Filippenko (1997) for a review, and Hook et al. (2005), Lidman et al. (2005), Matheson et al. (2005), and Howell et al. (2005) for issues associated with high-redshift SN classification. SNLS as a whole adopts the numerical classification scheme presented in Howell et al. (2005) for typing SNe: a confidence index (CI) that a given spectrum is of a SN Ia. Three classifications denote SNe Ia: "Certain SN Ia" (CI:5; type denoted as SN Ia), "Highly probable SN Ia" (CI:4; type denoted as SN Ia) and "Probable SN Ia" (CI:3; type denoted as SN Ia*). In all of the spectra in this paper, the relatively low-redshift compared to the SNLS sample as a whole, coupled with the long integration times, results in high signal-to-noise ratios ensuring the classifications are unambiguous. All SNe Ia presented here are CI=5 on the SNLS scheme.

3.3. Spectrophotometric Calibration and Host Galaxy Subtraction

Although standard spectrophotometric stars were observed periodically on each observing night, these provide only an approximation to a flux calibrated spectrum. Complexities such as differential slit-losses (as the seeing is wavelength dependent) and uncertain atmospheric extinction corrections require a more rigorous treatment. Furthermore, a key issue in the interpretation of SN spectra is the removal of underlying contaminating flux from the host galaxy, which for some high-redshift spectra can be significant. We adopted a procedure for removing the host galaxy spectrum that takes advantage of the photometric $u^\star g' r' i' z'$ host-galaxy data available from the SNLS, as well as the near-simultaneous SNLS $g' r' i' z'$ SN light-curve photometry, ensuring that each spectrum is carefully corrected to be consistent with the appropriate broad-band SN colors.

We begin by measuring the surface brightness of each galaxy (in flux units per square arcsecond) at the position of the SN in a series of small apertures (with radii of 1-8 pixels) for each of the $u^\star g' r' i' z'$ filters. These fluxes were measured from deep stacks with no SN light present, constructed for the purpose of studying the properties of the SN host galaxies (Sullivan et al. 2006b). The image quality of these stacks was around $0.8''$ in each filter, similar to the seeing for the majority of our LRIS spectral observations. The amount of host galaxy light present in each SN spectrum is then estimated by interpolating the galaxy surface brightnesses at the seeing of the observation, and then multiplying by the product

of the slitwidth (S_W) and the spectral extraction aperture (1.25×seeing; § 3.2), giving a series of $u^\star g'r'i'z'$ fluxes representing the host galaxy contamination in our spectra. We then fit a series of smooth galaxy spectral energy distribution (SED) templates to these flux data to estimate the contaminating host galaxy spectrum. These templates are generated by the galaxy spectral synthesis code PÉGASE.2 (Fioc & Rocca-Volmerange 1997, 1999) rebinned to the resolution of our SN spectra. We interpolate between neighboring galaxy spectra to find the best-fitting template. The resulting spectrum represents the estimate of the contaminating host galaxy continuum in every SN spectrum.

We next use the $g'r'i'z'$ SNLS light curves and their resulting light-curve parameterization (using the lightcurve fitter SiFTO; Conley et al., in prep) to interpolate the SN flux at the time of each spectral observation from nearby light-curve observations. Due to the rolling-search nature of the SNLS and the dense light curve coverage, most of the spectra in our main sample have g' photometric data within 2 rest-frame days of the spectroscopic observation, and all have data within 4 days (Table 1), hence the interpolation required is small.

We next estimate the amount of SN flux that went through the LRIS slit and was inside the spectral extraction window of 1.25×seeing, and hence is present in the reduced spectrum. We model the SN PSF as a two-dimensional Gaussian with σ = seeing/2.355 and integrate this Gaussian through an rectangular aperture of S_W×(seeing×1.25), where σ is calculated at the effective wavelengths of the $g'r'i'z'$ filters adjusting the seeing as $\lambda^{-0.2}$. This estimates the fraction of the total SN flux that passed through the slit, mimicking the inclusion of differential slit-losses. These adjusted SN fluxes are added to the host galaxy fluxes to generate combined "SN+host" $g'r'i'z'$ fluxes, the estimate of the amount of flux that passed through the slit.

We correct our combined, contiguous and flux-calibrated spectrum to have the same colors and absolute flux level as dictated by these "SN+host" fluxes using a smooth interpolating multiplicative spline function (see Hsiao et al. 2007). The size of the correction made to the observed spectrum is usually <10% and is invariably a monotonic function of wavelength. We then subtract our best-fitting host galaxy template, and adjust the resulting spectrum to have the correct colors of the SN on the night of observation (again using a spline function), giving a SN spectrum with the correct relative and absolute flux calibration. This final multiplicative adjustment is small and essentially corrects the subtracted spectrum for differential slit losses. We note that this technique would not be possible without either the $u^\star g'r'i'z'$ host galaxy fluxes, or the densely-sampled $g'r'i'z'$ SN Ia light curves.

We estimate the uncertainty in the host subtraction process using a Monte-Carlo simulation. We repeat the subtraction for each SN 500 times, but adjusting the different variables

(seeing, host-galaxy fluxes, SN fluxes) according to their uncertainties and assuming normal distributions. We assume a 15% uncertainty in the seeing, and also simulate errors in the centering of the SN in the slit, introduced during target acquisition or by telescope tracking errors, of $\pm 0.15''$ (1σ). Where appropriate, we use these 500 simulated spectra to estimate errors due to host galaxy subtraction in derived quantities (such as spectral colors) in later sections. We also carry forward in our analysis the statistical error arising from the photon statistics in our spectra (§ 3.2).

Our final task is to correct the SN Ia spectrum for the effects of extinction in the Milky-Way. To correct for Galactic extinction, we use the dust-maps of Schlegel, Finkbeiner, & Davis (1998) and a Cardelli, Clayton, & Mathis (1989) extinction law. We defer the more complex discussion of extinction in the SN host galaxy and intrinsic SN color variations until later.

We illustrate the results of this process for all 26 of our high quality SNe Ia in Fig. 2[3]

4. Methodology

We now turn to the two key questions our dataset is designed to address:

1. Has there been significant evolution in the mean SN Ia spectrum since $z \simeq 0.5$ - a period of 5 Gyr corresponding to the past 37% of cosmic history?

2. To what extent are there intrinsic spectral variations in our sample? Do these give indications that SNe Ia are a more complex population than assumed in cosmological studies, and might these variations limit the use of SNe Ia in future cosmology experiments?

4.1. Theoretical Predictions

We will begin to address these questions by exploring the role that our rest-frame UV data offers as a proxy for *progenitor metallicity*. The possible effects of progenitor metallicity, either as a function of redshift through galaxy evolution, or as a function of environment or host-galaxy luminosity, can be explored through blanketing and wavelength dependent features in the rest-frame UV corresponding to $\lambda\lambda$ 2900-3500Å. At z>0.2, this portion of

[3]The online version contains all spectra; the printed version contains two examples.

the rest-frame spectrum is well-sampled in our LRIS data. In making the assumption that our UV data are indicative of metallicity effects, it should be realized we are relying largely on theoretical studies; the UV spectral region is poorly explored observationally. First we review the various theoretical expectations.

Höflich, Wheeler, & Thielemann (1998) argue that direct traces of the progenitor metallicity can best be seen in the unburned SN layers which are only observable significantly before maximum light. However, they also predict that an increase in progenitor metallicity will cause an increase in the amount of ^{54}Fe synthesized in the explosion, and this will result in an increase in line opacity in the UV region which may be observable at maximum light. The degree of mixing in the explosion complicates the interpretation, however. The net effect predicted by Höflich et al. is that an increased metallicity will result in an *increase* in the UV pseudo-continuum at maximum light.

Lentz et al. (2000) start with the findings of Höflich et al. (1998) and examine the spectroscopic implications in greater detail. Using the starting isotopic distribution of the W7 model (Nomoto et al. 1984), they simultaneously change the progenitor metallicity in the unburned C+O region and increase the amount of ^{54}Fe in the partially burned region. They find two effects – a shift in the wavelength of UV features redward with decreasing metallicity, and a simultaneous increase in the level of the UV pseudo-continuum. They argue that as metallicity decreases so the line opacity decreases with the result that lines form deeper in the atmosphere, and therefore from a lower velocity region. A lower metallicity also decreases the cooling producing a higher temperature and bluer colors. We note that such a color difference is *opposite* to the effect predicted by Höflich et al. However, Lentz et al. caution that the overall UV flux level is not necessarily a good indicator of metallicity, as it is dependent on many variables such as the temperature, density and velocity of the C+O layer.

Timmes, Brown, & Truran (2003) argue for much more dramatic changes in SN Ia physics with metallicity. They argue that synthesized ^{56}Ni mass should be linearly proportional to progenitor metallicity. Since the decay of ^{56}Ni drives the luminosity, SNe Ia in high metallicity environments should be less luminous. This is because stars from higher metallicity environments will end up with larger mass fractions of ^{22}Ne and ^{56}Fe after helium burning. Since these isotopes have excess neutrons, the authors argue that in these cases fewer radioactive elements are produced during the process of burning to nuclear statistical equilibrium during a SN Ia. Note that these results are in sharp contrast to other studies which found no significant increase in ^{56}Ni with increasing metallicity (e.g. Höflich et al. 1998; Iwamoto et al. 1999)

Finally, we note that various authors predict that the SN Ia rate should be affected

by metallicity, although they do not make explicit predictions about the resulting effects on SN Ia properties. Kobayashi et al. (1998) argue that in very low metallicity environments ($[Fe/H] < -1$) the white dwarf wind that they believe is essential for producing SNe Ia will be inhibited, thus leading to fewer SNe Ia. Langer et al. (2000) find that metallicity differences should alter the range of progenitor masses that produce SNe Ia.

In summary therefore, theory cannot yet offer us a clear consensus as to the effects of metallicity on the UV properties of SNe Ia. Indeed, there is disagreement not only about which effects are the most important, but also about the sign of any possible effect. This is a very challenging theoretical problem hindered by correlations between the wanted effect of metallicity and other correlations such as the viability of certain progenitor systems, the explosion mechanism and radiative transfer in an atmosphere under a variety of mixing conditions. Full simulations of all these effects may soon become feasible, but substantial campaigns will still be needed to track statistical shifts with metallicity. We therefore undertake an empirically-motivated study of the properties of supernovae in the UV, and note where the observations agree or disagree with certain theoretical studies. In this respect, it is helpful to have some theoretical basis for making the empirical measures.

Fig. 3 illustrates, for the range of metallicities sampled by Lentz et al. (2000), that the bulk of the spectral changes would clearly be detectable within our rest-frame wavelength range. The blanketing and wavelength shifts apparent in Fig. 3 suggest the use of both photometric and spectroscopic diagnostics. As high quality UV spectra are in scarce supply at low redshift, we can best make meaningful comparisons using rest-frame $U - B$ measurements. As our spectra do not always extend to the full redward end of the standard B filter, we will also adopt a top-hat filter extending from 4000 to 4800Å which we will refer to as b. Pseudo-photometric ultraviolet measures can be constructed from our spectral data using two top-hat filters, UV1 and UV2, centered around regions where the strongest trends are predicted. Although these various photometric measures degrade the information content of our spectra, they have the considerable benefit of being consistent over a wide range in redshift without making any assumptions about the k-correction. The metallicity-induced spectral shifts discussed above can likewise be tracked by measuring the rest wavelengths of two UV features at $\lambda\lambda$2920 and 3180 Å . We will refer to these indicators as λ_1 and λ_2. Both the photometric and wavelength features introduced above are marked in Fig. 3.

4.2. Suitability of the Keck SNe Ia Sub-sample for Detailed Studies

If our conclusions concerning the properties of $z \simeq 0.5$ SNe Ia are to be relevant for the role of SNe Ia as cosmological probes, our sample of SNe Ia should be a representative

subset of those being used for probing dark energy. Accordingly, first we will verify whether this is the case by comparing the distribution of properties with those for the parent SNLS SN Ia sample. This parent sample (N=160) includes those presented by Astier et al. (2006), as well as further events up to May 2006, restricted to lie within our chosen redshift range $0.15< z <0.7$. This is the redshift range over which SNLS suffers least from Malmquist-type effects in the properties of SNe chosen for spectroscopic follow-up, and the broad SNLS population is reasonably unbiased over this redshift range (e.g. Astier et al. 2006; Neill et al. 2006).

Fig. 4 compares the distribution of SN Ia stretch, location and host galaxy properties for the two samples. There is no evidence that our selection criteria (§2) have significantly biased the SN Ia population chosen for intensive study relative to the larger SNLS population. Kolmogorov-Smirnov (K-S) tests indicate the Keck and SNLS sample distributions in all four parameters are consistent with being drawn from the same distribution; the exception is the stretch distribution where the K-S test indicates the distributions are possibly different due to a marginal deficiency of low stretch events in the Keck sample. This can be easily understood as these events are both fainter (making the Keck spectroscopic observations more demanding) and have faster light curves (making a pre-maximum or at maximum light observation less likely, a criterion when selecting SNe for Keck followup; § 2) than higher-stretch events. Otherwise, the larger scale environs in which our SNe Ia occurred seem quite representative of the parent population, for example in the specific star formation rate, the separation from the host galaxy, and (not shown in Fig. 4) the absolute magnitude of the host galaxy.

4.3. Local UV Spectra

In order to examine possible evolutionary effects we require a local baseline UV spectrum. For this, we turn to the analysis of Nugent, Kim, & Perlmutter (2002) which provides a phase-dependent template SN Ia spectrum which has become the standard reference used extensively, for example, in the calculation of cross-color k-corrections in deriving SNe Ia luminosities at high redshift. Further details of its construction can be found in the original article. Note that though improved spectral templates now exist (e.g. Guy et al. 2007; Hsiao et al. 2007), these typically exploit high-z spectra in their construction, whereas Nugent et al. use solely local SN Ia data.

The UV portion of this mean local spectrum is based on very few local events studied by either the IUE or HST (see Table 1 in Nugent et al. (2002)), and significant uncertainties remain at the shortest wavelengths. Unfortunately, unless STIS is resuscitated on the up-

coming HST Servicing Mission, there is no immediate prospect of improving this situation. A particular concern is the fact that within a week of peak brightness only three SN Ia (comprising of a total of five spectra) contribute to the UV template. They are SNe 1981B, 1990N and 1992A. These SNe have stretches of 0.929, 1.074 and 0.819 measured using SiFTO, i.e. within the range sampled here (Fig. 4). However, their hosts, classified as SAB(rs)bc (NGC 4536), SAB(rs)bc (NGC 4639) and SA0 (NGC 1380) respectively, are possibly biased towards large early type systems.

5. Results

5.1. Tests for Progenitor Evolution: the Mean UV SN Ia Spectrum

We begin by comparing the mean spectrum of the intermediate-redshift Keck SN Ia sample with the local Nugent et al. (2002) template. Earlier work comparing the properties of low and high-redshift SN Ia spectra (e.g. Coil et al. 2000; Hook et al. 2005; Blondin et al. 2006; Garavini et al. 2007; Bronder et al. 2007) has concentrated largely on comparisons of optical spectral features involving lower-S/N spectra. In general, these studies find that equivalent widths and ejection velocities of optical spectroscopic features measured on high-redshift SNe Ia have similar distributions to those observed locally. No study has yet found evidence for evolution in the optical spectroscopic properties of SNe Ia with redshift.

In this paper, we concentrate on the properties of the mean UV spectra. As discussed earlier, models suggest metallicity variations will have greatest effect in this wavelength region and thus our sensitivity to evolutionary effects should be maximized. We separate the distant SNLS events into three groups (Fig. 1): those observed prior to maximum light (t <-4 rest-frame days), those observed close to maximum light (-4< t <+4 days), and those observed after maximum light (t >+4 days). We exclude 3 spectra, labeled (f) in Table 1, which we classify as peculiar. One is the super-Chandrasekhar event SNLS-03D3bb (Howell et al. 2006) and the other two (SNLS-05D1hk and SNLS-03D4cj) have peculiar spectra similar to that of SN1991T-type (Filippenko et al. 1992). (A further 7 events, labeled (d-e) in Table 1, were discarded as described in § 2.) At this stage, our comparisons will involve spectra uncorrected for host galaxy extinction and/or intrinsic color variations.

Our 26 high-quality SNe Ia consist of 8 pre-max, 15 maximum light, and 3 post-max spectra. In creating a composite spectrum, flux-calibrated spectra are normalized using the top-hat b filter introduced earlier which runs from $\lambda\lambda$4000-4800Å (see Fig. 3). We use a clipped mean and determine the error on the mean by bootstrap resampling. To facilitate a meaningful comparison we color-adjust the local spectrum so that its $U-B$ color matches

that of the mean high redshift sample. Figs. 5 and 6 show the maximum-light and pre-maximum high-z mean spectra compared against the local template at similar phases. For convenience, we present in Tables 3 and 4, the early and maximum light spectral energy distributions with upper and lower 90% confidence limits. For the local template, due to the very small number of SNe Ia with rest-frame UV spectra (§ 4.3), a similar bootstrap resampling technique to asses the uncertainty in the local template is not meaningful.

Examining Fig. 5, it is clear that the spectrum at $\overline{z} \simeq 0.5$ is reasonably similar to its local equivalent. The agreement, particularly longward of 4000Å, is reassuring, indicating that there has been no significant evolution in the mean SN Ia spectroscopic properties over the past 5 Gyr. However, some systematic departures are seen, for example, in the Si II/Co II doublets at $\simeq$4150Å and in the positions of the UV features around 2900-3200Å.

Do these UV changes represent systematic differences in the progenitor properties between $z \simeq 0.5$ and 0? In this respect it is helpful to consider the error in the $z \simeq 0.5$ mean spectrum (shaded in Fig. 5). Here we see that the local spectrum lies within the 90% confidence boundary in the distribution of $z \simeq 0.5$ spectra. Thus it is quite possible that the UV differences seen between high and low redshift arise as a result of statistical variations occurring within a non-evolving population, especially considering the number of local SNe Ia with rest-frame UV coverage is very small.

Turning to the pre-maximum light spectra (Fig. 6), both Höflich et al. (1998) and Lentz et al. (2000) argue that differences in the UV spectrum due to changes in the progenitor metallicity should be larger at earlier times, where the unburned outer layers of the white dwarf play a larger role in shaping the appearance of the spectrum. Although the agreement does indeed seem to be poorer, the local template is considerably uncertain at this phase; we conclude that the most likely explanation for the differences we see is that the local template is unrepresentative in the far UV.

However, the differences that we do see in the UV data, whether due to evolution or simply as a result of intrinsic scatter in the population, are much larger than the effects predicted by Lentz et al. (2000) for quite substantial changes in progenitor metallicity. It should be noted that in these models, luminosity and kinetic energy were fixed, whereas our observations presumably span a considerable range in both of these variables. Lentz et al. also predict systematic wavelength shifts of the diagnostic features identified as λ_1 and λ_2 in Fig. 3, the study of which should be independent of reddening. We will defer consideration of these spectroscopic features until § 5.3.2.

At longer wavelengths, the local data is more reliable. Here, several features of the pre-maximum spectrum deserve comment (Fig. 6). Compared to the low-z template, the high-z

average spectrum has a shallower S II 5400Å feature, and a shallower Si II 4130Å feature. In addition the 3700Å Ca+Si feature is narrower and shows a greater degree of splitting into the separate Ca and Si components in the high-z composite spectrum. More high-z SNe Ia belong to what Branch et al. (2006) call the "shallow Si" group — SNe such as SN 1991T, which have a narrower zone of intermediate mass elements. These results agree with the findings of Li et al. (2001) who note that, while a significant fraction of SNe Ia show such behavior at early times, they become more normal at maximum light. This supports the claims of Sullivan et al. (2006b): at high redshift, where the fraction of star forming hosts is higher, more "prompt" SNe are found and these tend to have broader light curves.

The lack of a comprehensive local sample with comparable quality to the Keck data extending into the UV clearly limits any precise tests for spectral evolution. This impasse raises the question of whether it might be more profitable to search for evolutionary trends within the Keck sample itself. Fig. 7 shows the mean maximum light spectra compiled for two Keck sub-samples, split into two redshift ranges at z=0.50. The mean redshifts of the two subsamples are z=0.36 (N=7) and z=0.58 (N=8). The agreement is striking, with only marginal evidence for differences in blanketing at the shortest wavelengths. Further progress in this respect may be possible with the ongoing SDSS SN Ia survey (which samples $\overline{z} \simeq$0.2) and the higher-redshift SNLS SN Ia spectra at $z \simeq 0.6 - 1.0$.

In summary, no convincing evidence is available for a *systematic* change with redshift in the UV spectra of SNe Ia. The bulk of the differences seen probably arise from a natural dispersion within the sample and it seems reasonable to assume this dispersion is present at all epochs. In the next section we explore the possible origin of this UV dispersion.

5.2. Reality of the UV Dispersion

In this section we first consider the physical reality of the dispersion seen in the UV spectra at maximum light. The bootstrap-resampled variations (Figs. 5 and 6) indicate a greater degree of scatter at $\lambda < 3700$Å than in the optical around $\lambda \sim 5000$Å. However, both the effects of dust extinction and the size of the calibration uncertainties are unaccounted for in these comparisons. Could the increased dispersion simply arise as a result of one or both of these effects and not represent a true physical variation amongst our SNe?

We first discuss the effects of dust extinction.

5.2.1. Effects of Dust Extinction

An explanation for the UV variations is the presence of varying amount of interstellar dust, either in each host galaxy or along the line of sight to the observer. Correcting the properties of SNe Ia for extinction is currently one of the most pernicious problems in their use as cosmological probes (e.g., see discussion in Conley et al. 2007). Earlier analyses (Riess et al. 1996, 1998; Perlmutter et al. 1999; Riess et al. 2000; Sullivan et al. 2003; Knop et al. 2003), based on the first generation of SN Ia surveys, examined the range of likely extinction using both SN colors and host-galaxy morphologies as markers. Generally only modest levels of extinction ($A_V < 0^m.2$) were seen at high-redshift across the full range of host types, with no evidence of any systematic change with redshift in the samples used for cosmological analyses.

In the case of the present SNLS sample, the key diagnostic is the rest-frame $B-V$ color estimator "c" (Guy et al. 2005, 2007), essentially the $B-V$ color measured at maximum light. We wish to test whether dust is the primary cause of the UV variations seen in the Keck spectra. This can be done by considering, statistically, correlations between the UV spectra and c. Reddening measures for each SN are not directly output by the SNLS analysis since c is treated as an empirical variable when performing the cosmological analysis (Astier et al. 2006); no physical model is assumed for the color variations. However, we can readily test the hypothesis that the bulk of the UV dispersion arises from reddening that is linked to the $B-V$ variations.

We investigate two methods for color-correcting our SNe Ia spectra. The first is to use a standard reddening law (Cardelli et al. (1989), CCM) and extinction-correct each individual Keck spectrum using that SN's c measurement and a value of $R_B = 4.1$, suitable for standard Milky-Way type dust. The results from this process are not particularly sensitive to either the exact $B-V$ color used as the fiducial/zeropoint SN Ia color, nor to the exact value of R_B used. Our second approach is similar but uses the SALT (Guy et al. 2005) color law together with the c estimated from the light curve fits. As this color law was trained on local SN spectra and colors, it includes not only the effect of dust extinction but may also partially account for intrinsic variations between SN optical colors and UV fluxes unrelated to dust. The CCM and SALT laws have a similar form in the optical, but differ in the near-UV, where the SALT law implies more "extinction" in the UV than the CCM law (Guy et al. 2007). To test the validity of these approaches we split those Keck spectra studied at maximum light into two sub-samples according to whether the rest-frame maximum light optical color is redder or bluer than a c=-0.057.

Examining the mean UV spectra for the two subsets (Fig. 8), we find that, before any correction, optically bluer SNe Ia do indeed have more flux in the UV as expected if they are

less extincted. When the spectra are individually color-corrected using a CCM law and then combined by subset, the mean UV spectra agree better though the entire color difference is not corrected shortward of 3500Å. The approach using the SALT color law performs better in this UV region, and provides a good agreement across our entire wavelength range, but is unable to correct all the differences seen. Given the slightly superior performance of the SALT color law, we adopt this approach for color-correcting our spectra in the remainder of this paper.

5.2.2. Effects of Calibration Uncertainties

Our host galaxy subtraction and spectral calibration procedures are described in § 3.3. For each host-subtracted and photometrically-calibrated SN spectrum we also record a series of 500 Monte-Carlo simulated spectra generated by randomly varying the SN fluxes, host galaxy fluxes, seeing and SN position in the slit according to the observational errors.

For each of the SN studied, we estimate the 1-σ uncertainty as follows. In each wavelength bin for a given SN, we order the 500 random spectra and find the range in flux that encompasses 68% of the population and assign this flux range as the 1-σ error in this wavelength bin. This is repeated in every wavelength bin for all the spectra, providing the error from the observational uncertainties for each SN spectrum as a function of wavelength.

We can then assess whether the scatter that we see about the mean spectrum is significant. For every spectrum, we calculate the residual from the mean spectrum and divide by the appropriate error spectrum. The result is the deviation from the mean for each spectrum in units of sigma. Smoothed versions of these are plotted in Fig. 9; the top panel shows the deviation for the uncorrected spectra, the middle and lower panels show the deviations for spectra corrected using the CCM and SALT laws as described in § 5.2.1.

In general, the scatter is markedly larger in the UV ($\lambda < 4000$Å) than in the optical region. In the optical, the spectra appear well-behaved, with most of the deviations $<2\sigma$, consistent with a mean spectrum showing little intrinsic dispersion over the broad wavelength range.

These tests and those of the previous section demonstrate that most of the difference in the *average* continuum levels seen between the mean UV spectra of optically blue and red SNe Ia can be corrected using existing techniques such as the CCM dust extinction law or the SALT SN Ia color law. However, these techniques can only reduce, and not eliminate, the scatter observed, which is significantly larger than that expected from a consideration of the observational uncertainties. We thus conclude that the bulk of the dispersion is intrinsic

to our SNe and investigate its origin in the next sections.

5.3. Physical Correlations within the UV Dispersion

5.3.1. Photometric Comparisons

Given we have established that the UV variations are larger than those expected from photometric errors and are still present after attempts to correct for color differences, it is important to consider the extent to which the intrinsic dispersion we see is consistent or otherwise with that observed locally. Although no comparable local spectroscopic dataset exists, Jha et al. (2006) have analyzed a homogeneous photometric database of 44 local SNe Ia and examined the $U-B$ color dispersion at maximum light in terms of both the light curve stretch factor s and redder colors such as $B-V$. As in the higher redshift data, there is still the complication of separating the effects of host galaxy dust extinction and intrinsic color effects. In the Jha et al. study, host galaxy extinction estimates were available for a subset of the data yielding intrinsic $U-B$ and $B-V$ colors. The increased intrinsic dispersion seen in the $U-B$ vs. stretch relationship with respect to that in $B-V$ can thus be attributed primarily to an increased dispersion in the U band of $\sigma_U \simeq 0.12$ ($\simeq$12%).

Astier et al. (2006) also address the question of the intrinsic dispersion in U by comparing the photometric properties of that subset of SNLS SNe Ia for which some of the $g'r'i'z'$ bands map conveniently onto rest-frame UBV. They estimate the quantity ΔU_3 which is the difference between the U band flux at maximum light predicted from a suitably-chosen triplet of observed filters drawn from $g'r'i'z'$ and the actual observed U magnitude. As the machinery adopted by Astier et al. includes provision for a color-stretch relation, this is not quite the same test as that adopted by Jha et al., although the local scatter found in ΔU_3 is comparable (0.12).

We compare our intermediate redshift $U-b$-stretch relation with that derived from the local sample in Fig. 10. In this figure all colors are color-corrected using a SALT color law and the method of § 5.2.1. To derive the rest-frame $U-b$ and c measures for the low-z sample, we re-perform the light curve fits to the SN photometry using the same fitter used for the SNLS sample (SiFTO; Conley et al. in prep). Clearly, at maximum light the trends are very similar. As discussed in § 2, the Keck sample (and the SNLS sample in general) is slightly under-represented in low-stretch SNe Ia compared to the local data (Fig. 4), so the color-stretch relation found in previous studies is less evident. Crucially, there is no evidence that the colors derived directly from the Keck spectra show a larger photometric dispersion. For events with stretch s >0.85 we find $(U-b)$=-0.452 with a standard deviation

of 0.132 for 15 Keck SNe Ia c.f. -0.436 (0.167) for 41 local events. The small difference in mean color probably arises from the different selection criteria, as Jha et al. are able to include events with greater extinction. Note there are small differences in the definition of "maximum light"; the Keck spectra range over -4 to +4 days which will add an additional scatter to this sample in the presence of color evolution with phase.

A similar behavior is seen in the $(UV2-b)$ - stretch relation; a modest dispersion together with a weak correlation with stretch and a slight phase dependence (the definitions of UV1 and UV2 are shown in Fig.3). However, a marked increase in scatter is seen in the $(UV1-b)$ - stretch relation (as expected if the UV1 filter is the more sensitive to variations in progenitor composition) together with a stronger evolution with phase. Although the UV1 filter is the shortest wavelength probed by the Keck spectra, this dispersion is considerable even within a phase bin, and is unlikely to arise from spectrophotometric errors given the tight dispersion observed in the $UV2-b$ relation. Fig. 10 also shows weak correlations between color and stretch in the sense that the high stretch (brighter) events are bluer than those of low stretch (fainter) (e.g. Phillips et al. 1999; Knop et al. 2003; Garnavich et al. 2004).

Clearly as the SNe Ia develop they display an increased dispersion in the wavelength region where metal-dependent features are expected to be most prominent. This may indicate that the metallicity of the outer, unburned layers, seen only at early times, is not as important as expected by Höflich et al. (1998) and Lentz et al. (2000). Instead line blanketing from iron-peak elements may play the dominant role in affecting the UV opacity. This may affect maximum-light and post-maximum spectra more than for pre-maximum spectra. At early times the photosphere has not yet receded into the bulk of the iron-peak elements, and, as time progresses, ^{56}Ni synthesized in the explosion decays into ^{56}Co and subsequently into ^{56}Fe. These additional isotopes may provide the increased line blanketing seen in the spectra.

5.3.2. Spectroscopic Features

Next we consider trends in the spectroscopic features introduced by Lentz et al. (2000) as possible metallicity diagnostics; these are marked as λ_1 and λ_2 in Fig. 3. The wavelengths of these features have the advantage of being independent of any dust correction. If progenitor evolution is largely driven by metallicity effects, we might expect significant shifts to occur in these features between the local and high-redshift data.

In fact, a cursory examination of our mean spectra (Figs. 5 and 6) shows that the features do not appear to shift significantly in the mean. However this could be due to an inadequate or unrepresentative local data. We have seen that this is a significant limitation.

Accordingly, we measured the wavelength of both features for each of our spectra individually. For each feature we fit a Gaussian on a linear continuum background, returning the central wavelength. The error is estimated by varying the continuum definition either side of the feature, performing the fit 100 times, and taking the standard deviation of the resulting central wavelength distribution.

The precision is typically ±2-5Å, adequate to detect the shifts of ≃10Å predicted by Lentz et al. (2000). We found a much greater SN to SN scatter of ±60Å, with no obvious trend with stretch as might be expected from Fig. 10. However, as shown in Fig. 11, for both features there is a possible shift with phase in the sense both move gradually to longer wavelength as the SN expands. Moreover, there is a considerable dispersion at a particular phase, particularly before maximum light.

We find that λ_2 correlates reasonably well with the wavelength of the Si II 4130Å - a line commonly used to measure the photospheric expansion (Fig. 12). Thus, to first order, the scatter seen in λ_2 at a particular phase appears to arise from variations in kinetic energy within the sample. However the phase-dependent trend suggests a further process is at work. Fig. 13 shows the wavelength ratio versus phase, coded by stretch, where there is a noticeable shift at maximum light (corresponding to a redward shift of 50Å in λ_2). This shift presumably arises as a result of the effects of temperature and ionization changes which are more pronounced in the UV feature.

In summary, therefore, the above discussion suggests it will be very difficult to use these wavelength features as diagnostics of progenitor properties, unless perhaps larger samples are available. Clearly the analysis in Lentz et al. is oversimplified in several respects. Their models considered metallicity variations for a fixed luminosity and epoch, whereas it seems a wide range will be needed to isolate the effects of metallicity on this part of the spectrum. Recent work by Kasen & Woosley (2007), in which a grid of light curve models that span a large range in the production of ^{56}Ni and intermediate mass material (and hence overall kinetic energy), should provide an excellent starting place to address these factors in future work.

5.3.3. Host Galaxy and Stretch Dependences

In view of recent work using the SNLS (Sullivan et al. 2006b) where convincing correlations have been found between the properties of distant SNe Ia and their host galaxy environment, it is also natural to question whether the dispersion implied by the increased scatter in Fig. 10 is dependent on the stellar population and total stellar mass.

The Keck SN Ia dataset samples a wide range of passive and star-forming host galaxies (Fig. 4) for which stellar masses and luminosities are available (see Sullivan et al. 2006b, for details). Specific star formation rates and masses have been measured for the hosts using SED fits to the extracted colors with the Z-PEG photometric redshift code (Le Borgne & Rocca-Volmerange 2002).

In Fig. 14 we plot the color-corrected $UV1-b$ color against the host-galaxy stellar mass coding the data points according to whether the hosts are primarily passive or active. The discriminating specific star-formation rate was chosen to be 10^{-12} $M_{\odot}$ yr^{-1} per unit stellar mass (Fig. 4). Gas phase metallicities in star forming galaxies are well-known to correlate with galaxy mass (Tremonti et al. 2004; Kobulnicky et al. 2003) and recent studies have revealed these correlations were already in place at $z \simeq$1-1.5 (Shapley et al. 2005). Over the 3 dex range in stellar mass seen in our host galaxies, we would expect a change in metallicity of over 1 dex.

If, as Sullivan et al. surmise, the higher SN Ia rate in active hosts indicate the bulk of those SNe formed relatively recently, one might expect a tighter or different correlation between metallicity and galaxy mass than for those in passive galaxies. Unfortunately, Fig. 14 reveals an unavoidable difficulty with the modest Keck sample; our four passive galaxies are considerably more massive than most of the star-forming galaxies. Thus it is not straightforward to separate the effects of galaxy mass and specific star formation rate in understanding the implied metallicity dispersion. Nonetheless, to the extent we can examine any relationships, it seems there are much stronger trends between $UV1-b$ and inferred metallicity for SNe Ia in star-forming hosts than for those with passive hosts. At face value this would imply the most metal-rich progenitors have *less* UV blanketing. Clearly a larger sample will be needed to verify these trends. It may not be straightforward to sample lower-mass passive hosts, given fewer passive hosts are expected at high redshift in the hypothesis proposed by Sullivan et al..

A more informative comparison of the UV trends can be obtained by examining the spectra for those SNe Ia with high and low stretch. Although the host galaxy spectral class may contain events with a range of stretch (c.f. fig. 11 of Sullivan et al. (2006b)), such a categorization of events may be a more direct way of examining the spectral properties of events in old and young stellar populations (see also Bronder et al. 2007).

Fig. 15 shows the mean maximum-light SALT-law color-corrected spectra for those events with stretch s>1.03 and s$\leq$1.03. We also show the mean spectra split by s in the same way when the spectra are color-matched (rather than color-corrected) to have the same $U-b$ color. These comparisons confirm in detail the photometric trend noted in the rightmost panel of Fig. 10 – a strong and systematic difference in the far UV maximum-light

spectra of low and high-s SNe Ia.

As stretch (or light curve shape) maps closely onto both star-formation activity in the host galaxy (Sullivan et al. 2006b) and the morphology of the host galaxy (e.g. Hamuy et al. 2000), this comparison provides a clear example of the physical differences between SNe Ia in star forming and passive hosts and hence SNe Ia drawn from young and old stellar populations.

Clearly the mean spectrum of a SN Ia in a passive host with an old stellar population has a depressed far-UV continuum compared to one in a more active host with a younger stellar population even following color corrections based on optical colors. A broadly similar trend is observed by Guy et al. (2007). This is in the opposite sense than that expected from dust extinction, where the higher-stretch SNe Ia residing in spiral galaxies should suffer more extinction and therefore appear redder in the UV. Furthermore, the far-UV colors appear more sensitive to stretch than the optical colors.

Fig. 15 also reveals interesting differences between the optical spectral regions of high and low stretch supernovae. The majority of these differences originate due to the underlying temperature difference, with the high stretch supernovae showing stronger high excitation lines and ones from doubly-ionized elements. At $\simeq$4400 Å, a line due to Si III 4552 Å is found in the high stretch supernovae but is absent in the lower stretch examples. In addition, the 3700 Å Ca+Si feature is narrower and shows a greater degree of splitting into the separate Ca and Si components in the high stretch composite spectrum. Here one can also clearly see the difference between $\mathcal{R}$(Ca II) as defined in Nugent et al. (1995) where the ratio of the emission features on either side of this trough are greater in the low stretch composite. Finally, the Si II feature at 4130Å is shallower in high-stretch SNe consistent with trends identified by Bronder et al. (2007).

6. Discussion

One of the original motivations for this study was to explore both evolution in the mean properties of SNe Ia over $0< z <0.5$ and the dispersion in their UV spectra. We have seen remarkably little evidence of evolution in the mean spectroscopic properties over this interval, confirming, with higher precision, earlier suggestions based largely on lower-S/N data. The primary limitation in this aspect of our paper is the paucity of high quality UV data at low redshift.

Most of the earlier constraints on the possible evolution of SNe Ia were largely based on consideration of photometric measures. For example, Riess et al. (2004) derived the rest-

frame $U-B$ and $B-V$ distributions of a heterogeneous sample of SNe Ia at maximum light over z<1.5 as a proxy for the more precise constraints possible with spectroscopic data. They ruled out any color evolution greater than 0.02 mag in the mean in $U-B$.

Spectroscopic data is substantially more precise in its tracking of evolution and dispersion than broad-band photometry for two reasons. Foremost, detailed differences in key line diagnostics are lost in photometric data. Secondly, no assumptions need be made about k-corrections in gathering and comparing data over a broad redshift range.

At the time this Keck survey was underway, there was no comprehensive spectroscopic dataset against which our UV data could be compared, other than the mean template published by Nugent et al. (2002) and discussed in § 4.3. However, very recently, as a result of a survey of high-redshift SNe Ia with the ACS grism onboard Hubble Space Telescope, Riess et al. (2007) have published the mean rest-frame UV spectrum of 13 SNe Ia more distant ($z > 1$) than those studied here; the average redshift of this sample is $\overline{z}$=1.3. In this study, used to demonstrate the presence of dark energy at z >1, it is claimed that the sample-averaged spectral energy distributions observed at z >1 are consistent with that observed locally and that any spectral evolution is still undetected. However, no quantitative statement is made to support this claim.

We believe that the spectral comparison undertaken by Riess et al. (2007) is less precise than that undertaken in this study, and hence less valuable as a means of justifying the continued use of local relations in constructing SN Ia Hubble diagrams. Foremost, the ACS grism data samples SNe Ia over a much wider range of phase than the comparisons undertaken here. Although the individual spectra comprising the mean z=1.3 ACS spectrum are not tabulated by Riess et al. (2007), their phases range over at least 15-20 days and almost all are post-maximum light, compared with the narrow phase range maximum-light (-4 to +4 days) and pre-maximum light (<-4 days) comparisons presented here. A second consideration is the inevitable poor signal-to-noise ratio of these very high redshift spectra which precludes detailed comparisons.

As we have shown in Figs. 5 and 6, the local template (Nugent et al. 2002) is a poor basis from which to make such comparisons. More representative datasets are needed for reliable claims. Internally within our own data, Fig. 7 reveals little evolution although the redshift baseline is small. It will be important to examine the case for evolution from $0.2< z <1.5$ by combining in a consistent manner both the Riess et al. (2007) dataset with that presented here, as well as with higher-redshift SNLS SNe Ia (out to $z \sim 1$) observed during the routine survey spectroscopic screening (e.g. Bronder et al. 2007).

The second significant finding in this study is the marked increase in the dispersion

among our SNe Ia shortward of 3300Å (Fig. 10). Although the scatter in U is comparable to that seen in local data, it increases significantly at shorter wavelengths. Even allowing for differing amounts of dust extinction within each host galaxy, this amounts to more than a factor of 2 variation in continuum flux at maximum light. Although theoretical models predict a strong sensitivity to metallicity variations at this wavelength, our variations are also considerably larger than those predicted. We have demonstrated that a color correction based on the $B-V$ color of the SN and either a CCM Milky Way extinction law or a SALT color law, can only marginally reduce, and not eliminate, this UV dispersion.

We have found it hard to isolate the physical causes of this significant UV dispersion. We confirm earlier work at longer wavelengths ($\lambda \simeq$3500-4000Å) that shows that stretch (or equivalently host galaxy class) is partially responsible. However at the shortest wavelengths ($\lambda \simeq$3000-3300Å corresponding to our UV1 diagnostic), additional effects are clearly important that are not accounted for by the color-correction techniques in use in current cosmological programs. In addition to the newly-found intrinsic scatter at short wavelengths, new trends with phase are also seen in the wavelengths of diagnostic features in this region.

Redward of 4000 Å , corrections for stretch or color work well in normalizing SNe Ia, however blueward of 4000A, significant scatter remains even after such corrections are made. This may be related to a change in the dominant source of opacity in SNe Ia. Redward of 3500-4000 Å electron scattering opacity dominates, but at UV wavelengths a forest of overlapping lines is the dominant source of opacity (see Fig. 1 of Hillebrandt & Niemeyer (2000)). Electron scattering is a continuous process involving well-understood physics, but line opacity depends sensitively on abundances, ionization states, and possibly non-LTE effects.

Fig. 16 illustrates this point by comparing the wavelength dependence of the line and electron scattering opacity at maximum light for a model by Kasen & Woosley (2007) that provides a good match for a normal SN Ia (Kason, priv. commun.). The data in question refers to that at a depth of 7000 $\mathrm{km\,s^{-1}}$ where intermediate mass and Fe peak material are well-mixed. A common feature in these models is the drop in line opacity compared to the electron scattering opacity near 4000 Å as seen here. Thus it is understandable that the emerging UV flux is highly susceptible to changes in the line opacity (due to initial conditions and/or material synthesized during the explosion) while the optical and near-IR spectral behavior are dominated by electron scattering opacity at this phase.

What are the possible consequences of the above variations in terms of the use of SNe Ia as probes of the expansion history? In the highest redshift surveys, including those proposed with future facilities, cross-color k-corrections are needed to estimate rest-frame light curves from the observations, typically undertaken in the far-red and near-infrared for $z >$1.5 (Riess

et al. 2004, 2007). This necessitates the adoption of a suitable template whose SED is reliable in the 3000-4000Å region. At the most fundamental level, the dispersion in our UV spectra will contribute a statistical uncertainty at the 0.05-0.1 magnitude level depending on how precisely particular observed filters match to the chosen rest-frame bandpasses.

A more worrying bias would follow the adoption of an incorrect template. Possibly the most significant finding in our work is the demonstration that the mean UV spectrum is different for high and low stretch SNe Ia (Fig. 15) and thus, presumably, for those that occur in passive and actively star-forming galaxies (Sullivan et al. 2006b). Adopting a single template would lead to a systematic bias which could become increasingly serious at high redshift where the mix between the two populations changes and high-stretch SNe, typically originating from younger progenitor systems, become increasingly common. Recently, Howell et al. (2007) have demonstrated the existence of an increased fraction of high-stretch SNe Ia at higher redshifts above and beyond the selection effect that high stretch, brighter SNe Ia are easier to detect.

Using our individual maximum light spectra, we can evaluate the impact of the UV dispersion on sample cross-color k-corrections, addressing both the statistical error arising from the intrinsic scatter and the systematic difference arising from the stretch-based spectral differences we have found. Fig. 17 shows the result.

For a typical future dark energy experiment, based on securing the equation of state parameter w to 5% using z >1 SNe Ia, photometric corrections of better than ±0.02 mag are required [4]. This requirement is indicated on Fig. 17.

In terms of the *statistical* error, the observed dispersion is typically ±0.05-0.10 mag, larger than that required by a factor of several. However, such a dispersion, if randomly distributed, need not present a fundamental obstacle to progress with a survey spanning a wide redshift range utilizing a large number of SNe Ia. As Fig. 17 shows, at certain redshifts where the rest-frame and observed filters closely match, the dispersion has negligible effect and SNe Ia at these redshifts could be more heavily weighted.

The more worrying trend, particularly given the recent demonstration of stretch bias by Howell et al. (2007), is the likelihood of a *systematic* error introduced by adopting an incorrect template for the redshifts where the rest-frame and observed filters do not overlap. Fig. 17 shows the potential of this error via a comparison of the dispersion independently for high and low stretch events. The differences between these two categories are comparably

[4]e.g. White Papers submitted to the US Dark Energy Task Force Committee: http://www.nsf.gov/mps/ast/detf.jsp

large and indicate the importance of securing a physical understanding of the UV variations seen in our survey.

7. Conclusions

We summarize our findings as follows:

1. We have secured high signal-to-noise ratio Keck spectra for a sample of 36 intermediate redshift SNe Ia, observed at various phases, spanning the redshift range $0.15< z <0.7$, and drawn from the Supernova Legacy Survey (SNLS). We demonstrate via inspection of the SN properties that our Keck sample is a reasonably fair subset of the larger sample of distant SNe Ia being studied by the SNLS.

2. We develop a new method for removing host galaxy contamination from our spectra based on measures of the galaxy and SN photometry. These refinements to traditional spectral reduction techniques allow us to achieve host-galaxy subtracted and flux-calibrated rest-frame spectra of high quality, extending down to rest-frame wavelengths of 2900Å.

3. Although no strong evidence is found for spectral evolution in the mean early-phase and maximum light spectra, when compared to local data, such evolutionary tests are hampered by the paucity of quality data at low redshift and a significant scatter in the spectra shortward of 4000Å. We find no evidence for evolution internal to our data. We argue that the well-used local UV spectral template (Nugent et al. 2002) is likely to be less representative than the mean spectrum compiled from the Keck data which we tabulate with the measured dispersion for use in future cosmological applications.

4. Our principal finding is a large scatter from one SN to the next in the rest-frame UV spectrum even after standard dust corrections are made. By constructing various photometric bandpasses that avoid uncertainties arising from differential k-corrections associated with the range of redshifts in our sample, we show that while we can reproduce the stretch-dependent trends seen locally at 3500-4000Å, the scatter at 3000-3400Å is 3-5 times larger.

5. Although progenitor metallicity may drive some of the trends seen in the Keck data, the UV variations are much larger than in contemporary models which span the expected metallicity range. Moreover, the UV spectrum also changes with phase in a manner which is not consistent with models. We conclude there are significant variations in the

UV properties of SNe Ia which are not accounted for by either the presently-employed empirical trends or the available SN Ia models.

6. As an illustration of the importance of understanding these new results, we calculate the error arising from the use of a single UV spectral template for calculating the cross-color k correction, a correction essential for constructing the SN Ia Hubble diagram as a probe of the expansion history. The dispersion arising from our UV spectra, if not randomly distributed along the Hubble diagram, presents an uncertainty 2-3 times larger than than would be necessary for recovering the equation of state parameter w to 5% using SNe Ia at $z \simeq 1$. We conclude that further detailed studies are essential if SNe Ia are to be useful for precision measures of dark energy.

The spectroscopic data presented herein were obtained at the W.M. Keck Observatory, which is operated as a scientific partnership among the California Institute of Technology, the University of California and the National Aeronautics and Space Administration. The Observatory was made possible by the generous financial support of the W.M. Keck Foundation. The authors wish to recognize and acknowledge the very significant cultural role and reverence that the summit of Mauna Kea has always had within the indigenous Hawaiian community. We are most fortunate to have the opportunity to conduct observations from this mountain. Additional observations were obtained with MegaPrime/MegaCam, a joint project of CFHT and CEA/DAPNIA, at the Canada-France-Hawaii Telescope which is operated by the National Research Council (NRC) of Canada, the Institut National des Sciences de l'Univers of the Centre National de la Recherche Scientifique (CNRS) of France, and the University of Hawaii. Canadian collaboration members acknowledge support from NSERC and CIAR; French collaboration members from CNRS/IN2P3, CNRS/INSU and CEA. PEN acknowledges support from the US Department of Energy Scientific Discovery through Advanced Computing program under contract DE-FG02-06ER06-04. A.G. acknowledges support by NASA through Hubble Fellowship grant #HST-HF-01158.01-A awarded by STScI, which is operated by AURA, Inc., for NASA, under contract NAS 5-26555. RSE acknowledges financial support from DOE under contract DE-FG02-04ER41316. This research used resources of the National Energy Research Scientific Computing Center, which is supported by the Office of Science of the U.S. Department of Energy under Contract No. DE-AC02-05CH11231. We thank them for a generous allocation of computing time. We acknowledge useful discussions with Adam Riess, Mario Livio, and Ken Nomoto.

Facilities: Keck:I, CFHT.

REFERENCES

Aldering, G. 2005, New Astronomy Review, 49, 346

Aldering, G., et al. 2002, in Survey and Other Telescope Technologies and Discoveries. Edited by Tyson, J. Anthony; Wolff, Sidney. Proceedings of the SPIE, Volume 4836, pp. 61-72 (2002)., 61–72

Astier, P., et al. 2006, A&A, 447, 31

Benford, D. J., & Lauer, T. R. 2006, in Presented at the Society of Photo-Optical Instrumentation Engineers (SPIE) Conference, Vol. 6265, Space Telescopes and Instrumentation I: Optical, Infrared, and Millimeter. Edited by Mather, John C.; MacEwen, Howard A.; de Graauw, Mattheus W. M.. Proceedings of the SPIE, Volume 6265, pp. 626528 (2006).

Bessell, M. S. 1990, PASP, 102, 1181

Blondin, S., et al. 2006, AJ, 131, 1648

Boulade, O., et al. 2003, in Instrument Design and Performance for Optical/Infrared Groundbased Telescopes. Edited by Iye, Masanori; Moorwood, Alan F. M. Proceedings of the SPIE, Volume 4841, pp. 72-81 (2003)., 72–81

Branch, D., et al. 2006, PASP, 118, 560

Bronder, J. B., et al. 2007, in A&A, accepted

Cappellaro, E., Turatto, M., & Fernley, J. 1995, ESA SCIENTIFIC PUBLICATION ESA-SP 1189, 1189

Cardelli, J. A., Clayton, G. C., & Mathis, J. S. 1989, ApJ, 345, 245

Coil, A. L., et al. 2000, ApJ, 544, L111

Cole, S., et al. 2005, MNRAS, 362, 505

Conley, A., Carlberg, R. G., Guy, J., Howell, D. A., Jha, S., Riess, A. G., & Sullivan, M. 2007, ArXiv e-prints, 705

Efstathiou, G., et al. 2002, MNRAS, 330, L29

Eisenstein, D. J., et al. 2005, ApJ, 633, 560

Filippenko, A. V. 1982, PASP, 94, 715

—. 1997, ARA&A, 35, 309

Filippenko, A. V., et al. 1992, ApJ, 384, L15

Fioc, M., & Rocca-Volmerange, B. 1997, A&A, 326, 950

—. 1999, ArXiv Astrophysics e-prints

Gallagher, J. S., Garnavich, P. M., Berlind, P., Challis, P., Jha, S., & Kirshner, R. P. 2005, ApJ, 634, 210

Garavini, G., et al. 2007, A&A, 470, 411

Garnavich, P. M., et al. 2004, ApJ, 613, 1120

Guy, J., et al. 2007, A&A, 466, 11

Guy, J., Astier, P., Nobili, S., Regnault, N., & Pain, R. 2005, A&A, 443, 781

Höflich, P., Wheeler, J. C., & Thielemann, F. K. 1998, ApJ, 495, 617

Hamuy, M., et al. 2006, PASP, 118, 2

Hamuy, M., Phillips, M. M., Maza, J., Suntzeff, N. B., Schommer, R. A., & Aviles, R. 1995, AJ, 109, 1

Hamuy, M., Trager, S. C., Pinto, P. A., Phillips, M. M., Schommer, R. A., Ivanov, V., & Suntzeff, N. B. 2000, AJ, 120, 1479

Hillebrandt, W. & Niemeyer, J.-C. 2000, ARA&A, 38, 191

Hook, I. M., et al. 2005, AJ, 130, 2788

Howell, D. A. 2001, ApJ, 554, L193

Howell, D. A., Sullivan, M., Conley, A., & Carlberg, R. 2007, ArXiv Astrophysics e-prints

Howell, D. A., et al. 2006, Nature, 443, 308

Howell, D. A., et al. 2005, ApJ, 634, 1190

Howell, D. A., Wang, L., Supernova Cosmology Project Collaboration, & Supernova Factory Collaboration. 2002, Bulletin of the American Astronomical Society, 34, 1256

Hsiao, E. Y., Conley, A., Howell, D. A., Sullivan, M., Pritchet, C. J., Carlberg, R. G., Nugent, P. E., & Phillips, M. M. 2007, ApJ, 663, 1187

Iwamoto, K., Brachwitz, F., Nomoto, K., Kishimoto, N., Umeda, H., Hix, W. R., & Thielemann, F.-K. 1999, ApJS, 125, 439

Jha, S., et al. 2006, AJ, 131, 527

Kasen, D., & Woosley, S. E. 2007, ApJ, 656, 661

Kelson, D. D. 2003, PASP, 115, 688

Kirshner, R. P., et al. 1993, ApJ, 415, 589

Knop, R. A., et al. 2003, ApJ, 598, 102

Kobayashi, C., Tsujimoto, T., Nomoto, K., Hachisu, I., & Kato, M. 1998, ApJ, 503, L155

Kobulnicky, H. A., et al. 2003, ApJ, 599, 1006

Krisciunas, K., et al. 1987, PASP, 99, 887+

Langer, N., Deutschmann, A., Wellstein, S., & Höflich, P. 2000, A&A, 362, 1046

Le Borgne, D., & Rocca-Volmerange, B. 2002, A&A, 386, 446

Leibundgut, B., Kirshner, R. P., Filippenko, A. V., Shields, J. C., Foltz, C. B., Phillips, M. M., & Sonneborn, G. 1991, ApJ, 371, L23

Lentz, E. J., Baron, E., Branch, D., Hauschildt, P. H., & Nugent, P. E. 2000, ApJ, 530, 966

Li, W., & Filippenko, A. V. 2005, in IAU Colloq. 192: Cosmic Explosions, On the 10th Anniversary of SN1993J, ed. J.-M. Marcaide & K. W. Weiler, 525–+

Li, W., Filippenko, A. V., Treffers, R. R., Riess, A. G., Hu, J., & Qiu, Y. 2001, ApJ, 546, 734

Lidman, C., et al. 2005, A&A, 430, 843

Mannucci, F., Della Valle, M., & Panagia, N. 2006, MNRAS, 370, 773

Mannucci, F., della Valle, M., Panagia, N., Cappellaro, E., Cresci, G., Maiolino, R., Petrosian, A., & Turatto, M. 2005, A&A, 433, 807

Massey, P., Strobel, K., Barnes, J. V., & Anderson, E. 1988, ApJ, 328, 315

Matheson, T., et al. 2005, AJ, 129, 2352

Neill, J. D., et al. 2006, AJ, 132, 1126

Nugent, P., Phillips, M., Baron, E., Branch, D., & Hauschildt, P. 1995, ApJ, 455, L147

Nugent, P., Kim, A., & Perlmutter, S. 2002, PASP, 114, 803

Nugent, P., et al. 2006, ApJ, 645, 841

Oke, J. B., et al. 1995, PASP, 107, 375

Perlmutter, S., et al. 1999, ApJ, 517, 565

Perlmutter, S., et al. 1997, ApJ, 483, 565

Phillips, M. M., Lira, P., Suntzeff, N. B., Schommer, R. A., Hamuy, M., & Maza, J. . 1999, AJ, 118, 1766

Riess, A. G., et al. 1998, AJ, 116, 1009

Riess, A. G., et al. 2000, ApJ, 536, 62

Riess, A. G., et al. 1999, AJ, 117, 707

Riess, A. G., Press, W. H., & Kirshner, R. P. 1996, ApJ, 473, 88

Riess, A. G., et al. 2004, ApJ, 607, 665

Riess, A. G., et al. 2007, ApJ, 659, 98

Scannapieco, E., & Bildsten, L. 2005, ApJ, 629, L85

Schlegel, D. J., Finkbeiner, D. P., & Davis, M. 1998, ApJ, 500, 525

Schmidt, B. P., et al. 1998, ApJ, 507, 46

Shapley, A. E., Coil, A. L., Ma, C.-P., & Bundy, K. 2005, ApJ, 635, 1006

Spergel, D. N., et al. 2007, ApJS, 170, 377

Sullivan, M., et al. 2003, MNRAS, 340, 1057

Sullivan, M., et al. 2006a, AJ, 131, 960

Sullivan, M., et al. 2006b, ApJ, 648, 868

Timmes, F. X., Brown, E. F., & Truran, J. W. 2003, ApJ, 590, L83

Tremonti, C. A., et al. 2004, ApJ, 613, 898

van Dokkum, P. G. 2001, PASP, 113, 1420

Wood-Vasey, W. M., et al. 2007, ApJ, 666, 694

This preprint was prepared with the AAS LaTeX macros v5.2.

Table 1. Distant Supernova Sample

SN Name[a]	RA (J2000)	DEC (J2000)	Redshift	Phase (Days)[b]	Stretch	Nearest g' phot (Days)[b]	% Inc.[c]	Redshift Source
03D1au	02:24:10.38	-04:02:14.9	0.5043 ± 0.0005	-1.6 ± 0.3	1.14 ± 0.02	+0.6	432	Galaxy
03D1aw	02:24:14.78	-04:31:01.6	0.582 ± 0.005	$+2.4 \pm 0.3$	1.08 ± 0.02	+0.6	856	Galaxy
03D1co	02:26:16.23	-04:56:05.7	0.679 ± 0.001	$+7.1 \pm 0.5$	1.07 ± 0.04	+0.7	321	Galaxy
03D1dj	02:26:19.08	-04:07:09.3	0.40 ± 0.01	-1.8 ± 2.3	1.25 ± 0.61	+0.1	4199	Template Fit
03D3af	14:21:14.92	+52:32:15.3	0.5320 ± 0.0005	$+2.8 \pm 0.4$	1.02 ± 0.03	+3.8	368	Galaxy
03D3aw[e]	14:20:53.61	+52:36:20.6	0.449 ± 0.001	-0.8 ± 0.2	0.94 ± 0.03	-13.7	52	Galaxy
03D3ay[e]	14:17:58.43	+52:28:57.4	0.3709 ± 0.0003	-1.0 ± 0.2	1.00 ± 0.03	-14.6	72	Galaxy
03D3ba[e]	14:16:33.44	+52:20:32.1	0.2912 ± 0.0003	$+12.8 \pm 0.4$	1.04 ± 0.03	-15.5	259	Galaxy
03D3bb[f]	14:16:18.78	+52:14:55.3	0.2437 ± 0.0003	$+2.2 \pm 0.3$	1.18 ± 0.03	-16.2	2323	Galaxy
03D3bh[e]	14:21:35.89	+52:31:37.6	0.2486 ± 0.0003	-3.5 ± 0.2	1.02 ± 0.03	-16.1	140	Galaxy
03D3bl	14:19:55.90	+53:05:51.0	0.3553 ± 0.0005	$+3.7 \pm 0.5$	0.98 ± 0.03	-0.1	270	Galaxy
03D3cc	14:19:45.25	+52:32:25.3	0.4627 ± 0.0003	$+8.5 \pm 0.4$	1.04 ± 0.02	-0.1	204	Galaxy
03D3cd	14:18:39.95	+52:36:43.8	0.4607 ± 0.0005	-5.6 ± 0.1	1.15 ± 0.02	-0.1	625	Galaxy
03D4ag	22:14:45.79	-17:44:23.0	0.2847 ± 0.0003	-5.0 ± 0.1	1.08 ± 0.02	-1.6	141	Galaxy
03D4cj[f]	22:16:06.66	-17:42:16.7	0.27 ± 0.01	-7.4 ± 0.1	1.09 ± 0.01	+1.5	5000	Template Fit
03D4dh	22:17:31.04	-17:37:46.9	0.6268 ± 0.0004	$+0.5 \pm 0.3$	1.08 ± 0.02	+0.6	444	Galaxy
03D4gl[e]	22:14:44.17	-17:31:44.4	0.571 ± 0.001	$+7.7 \pm 0.5$	1.00 ± 0.03	+14.6	347	Galaxy
04D1hd	02:26:08.85	-04:06:35.2	0.3688 ± 0.0004	$+1.6 \pm 0.1$	1.06 ± 0.01	+1.4	1998	Galaxy
04D1jg	02:26:12.56	-04:08:05.3	0.5842 ± 0.0005	-2.0 ± 0.2	1.05 ± 0.02	+1.3	128	Galaxy
04D1oh[d]	02:25:02.37	-04:14:10.5	0.59 ± 0.01	-6.0 ± 0.2	1.03 ± 0.02	+0.1	512	Template Fit
04D1rh	02:27:47.16	-04:15:13.6	0.4349 ± 0.0005	$+2.6 \pm 0.3$	1.02 ± 0.03	-0.1	393	Galaxy
04D1sk	02:24:22.77	-04:21:13.3	0.6634 ± 0.0005	-0.4 ± 0.6	0.86 ± 0.04	+0.0	139	Galaxy
04D2gc	10:01:39.26	+01:52:59.5	0.5216 ± 0.0005	-0.2 ± 0.3	1.14 ± 0.03	-0.9	367	Galaxy
04D2kr	10:00:37.32	+01:42:43.1	0.7441 ± 0.0005	-2.5 ± 0.6	1.06 ± 0.04	+0.6	91	Galaxy
04D3cp[d]	14:20:23.95	+52:49:15.5	0.83 ± 0.02	$+5.2 \pm 0.4$	1.07 ± 0.02	+0.5	557	Galaxy
04D3ez	14:19:07.91	+53:04:18.8	0.2630 ± 0.0005	$+1.6 \pm 0.1$	0.92 ± 0.02	-0.4	78	Galaxy
04D3fk	14:18:26.21	+52:31:42.7	0.3578 ± 0.0007	-6.9 ± 0.1	0.97 ± 0.01	-0.4	136	Galaxy
04D4in	22:15:08.58	-17:15:39.8	0.5160 ± 0.0005	-4.6 ± 0.1	1.13 ± 0.01	+2.0	443	Galaxy
04D4jr	22:14:14.33	-17:21:00.9	0.482 ± 0.007	-0.2 ± 0.2	1.16 ± 0.02	+2.7	5000	Template Fit
05D1hk[f]	02:24:39.16	-04:38:03.0	0.2631 ± 0.0002	-8.6 ± 0.1	1.16 ± 0.01	-0.8	337	Galaxy
05D1hn	02:24:36.25	-04:10:54.9	0.1489 ± 0.0006	-7.2 ± 0.1	1.06 ± 0.02	-0.8	232	Galaxy
05D1if	02:24:29.71	-04:34:13.0	0.763 ± 0.001	-5.0 ± 0.3	1.03 ± 0.03	-0.0	5000	Galaxy
05D1ix	02:24:19.95	-04:40:11.7	0.49 ± 0.01	-8.7 ± 0.2	1.05 ± 0.01	-0.7	5000	Template Fit
05D1iy	02:27:39.97	-04:25:21.3	0.2478 ± 0.0003	-9.2 ± 0.1	0.88 ± 0.01	-0.7	52	Galaxy
05D2le	10:01:54.85	+02:05:34.7	0.7002 ± 0.0005	$+6.3 \pm 0.4$	1.10 ± 0.04	-0.0	2647	Galaxy
05D2mp	09:59:08.61	+02:12:14.6	0.3537 ± 0.0004	-3.9 ± 0.2	1.11 ± 0.02	+0.7	831	Galaxy

[a]The SNLS ID format is explained in Howell et al. (2005); briefly, it relates to the year of discovery (03, 04 etc.), the relevant SNLS field (D1 through D4), and a running ID (e.g. aa, ab, ac etc.).

[b]"Effective" rest-frame phase relative to maximum light i.e. $(T_{\rm obs} - T_{\rm max})/(s \times (1+z))$

[c]Estimated through the spectral extraction aperture; increases greater than 5000% are listed as 5000%.

[d]ight curve deemed inadequate in temporal coverage.

[e]Spectrum deemed inadequate in signal-to-noise ratio.

[f]Spectroscopically peculiar; excluded from primary analysis sample.

Table 2. Observing log

SN Name	Date Obs	MJD	Seeing (″)	Slit (″)	Dichroic	Exptime (s)	SN apparent i' mag.
03D1au	2003-09-23	52905.51	0.8	1.0	560	5400	22.4
03D1aw	2003-09-23	52905.58	0.8	1.0	560	5400	22.7
03D1co	2003-11-22	52965.48	0.9	1.0	680	9000	23.5
03D1dj	2003-11-21	52964.47	0.8	1.0	560	6000	22.0
03D3af	2003-04-07	52736.41	0.9	1.0	680	5400	22.7
03D3aw	2003-05-06	52765.53	0.9	1.0	680	4800	22.2
03D3ay	2003-05-06	52765.47	0.9	1.0	680	3600	21.7
03D3ba	2003-05-06	52765.38	0.9	1.0	680	3600	21.7
03D3bb	2003-05-06	52765.29	0.9	1.0	560	2000	19.8
03D3bh	2003-05-06	52765.32	0.9	1.0	560	3600	20.9
03D3bl	2003-06-01	52791.33	0.9	1.0	680	3600	22.0
03D3cc	2003-06-02	52792.27	1.0	1.0	680	5400	22.1
03D3cd	2003-06-01	52791.27	1.0	1.0	680	9777	22.2
03D4ag	2003-07-02	52822.54	0.9	1.0	560	5400	21.1
03D4cj	2003-08-27	52878.32	0.9	1.0	560	4000	21.2
03D4dh	2003-09-23	52905.43	0.8	1.0	560	3600	22.6
03D4gl	2003-11-22	52965.26	0.9	1.0	680	7200	22.6
04D1hd	2004-09-21	53269.47	0.9	1.0	560	6000	21.6
04D1jg	2004-09-21	53269.56	0.9	1.0	560	6000	22.5
04D1oh	2004-10-19	53297.54	1.0	1.0	560	7200	22.9
04D1rh	2004-12-14	53353.24	0.9	0.7	560	6000	21.9
04D1sk	2004-12-14	53353.36	0.9	1.0	560	9000	23.2
04D2gc	2004-04-22	53117.00	0.7	0.7	560	6600	22.5
04D2kr	2004-12-14	53353.58	0.9	1.0	560	9600	22.8
04D3cp	2004-04-23	53118.45	0.8	0.7	560	2700	23.1
04D3ez	2004-04-22	53117.00	0.8	0.7	560	3600	21.0
04D3fk	2004-04-22	53117.00	0.8	0.7	560	4500	22.3
04D4in	2004-09-21	53269.31	0.9	1.0	560	7200	22.4
04D4jr	2004-10-19	53297.28	1.0	1.0	560	7200	22.0
05D1hk	2005-11-30	53704.37	0.9	1.0	560	2400	21.5
05D1hn	2005-11-30	53704.40	0.9	1.0	560	2100	20.8
05D1if	2005-12-01	53705.31	0.9	1.0	560	9000	23.2

Table 2—Continued

SN Name	Date Obs	MJD	Seeing (″)	Slit (″)	Dichroic	Exptime (s)	SN apparent i' mag.
05D1ix	2005-11-30	53704.28	0.9	1.0	560	7200	22.9
05D1iy	2005-11-30	53704.43	0.9	1.0	560	4800	22.1
05D2le	2005-12-01	53705.57	0.9	1.0	560	7200	23.2
05D2mp	2005-11-30	53704.53	0.9	1.0	560	6600	21.9

Table 3. Mean SN Ia spectrum (Early)

Wavelength (Å)	Flux	Flux lower	Flux upper
2805	0.506	0.302	0.629
2810	0.579	0.322	0.643
2815	0.417	0.364	0.662
2820	0.477	0.390	0.682
2825	0.482	0.431	0.708
2830	0.529	0.449	0.724
2835	0.747	0.472	0.757
2840	0.723	0.483	0.792
2845	0.676	0.481	0.813
2850	0.719	0.495	0.830

Note. — The complete version of this table is in the electronic edition of the Journal. The printed edition contains only a sample.

Table 4. Mean SN Ia spectrum (Max)

Wavelength (Å)	Flux	Flux lower	Flux upper
2805	0.287	0.262	0.411
2810	0.360	0.282	0.422
2815	0.372	0.299	0.435
2820	0.438	0.317	0.448
2825	0.355	0.334	0.456
2830	0.477	0.349	0.470
2835	0.433	0.357	0.472
2840	0.378	0.367	0.483
2845	0.442	0.375	0.496
2850	0.428	0.377	0.506

Note. — The complete version of this table is in the electronic edition of the Journal. The printed edition contains only a sample.

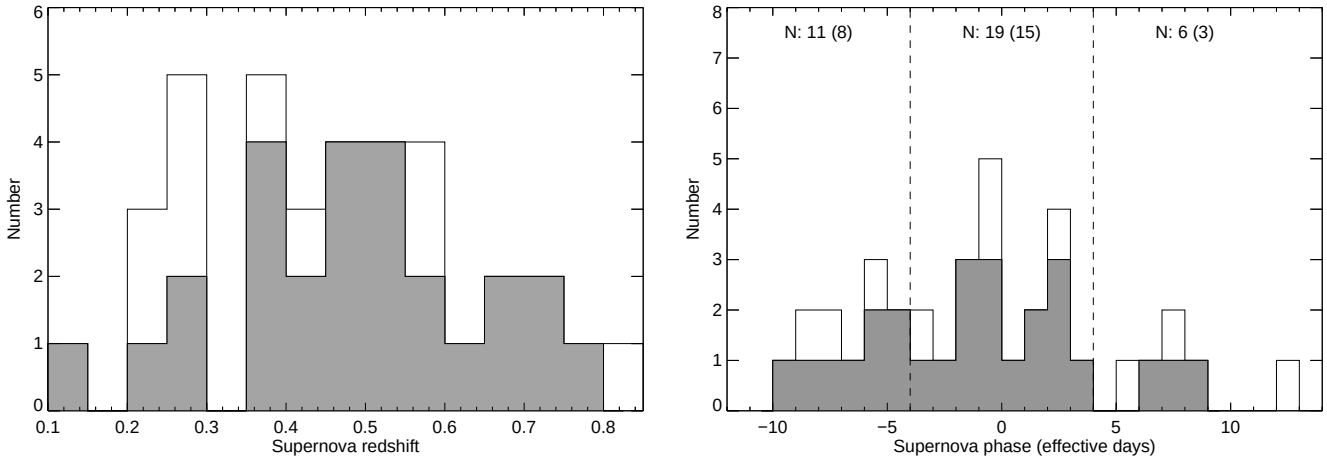

Fig. 1.— Redshift (left) and phase (right) distributions of the high-redshift SNLS SNe Ia studied in this paper. The vertical dashed lines in the phase distributions show how the SN Ia sample is divided into "early" and "maximum-light" spectra. Numbers (and the open histograms) refer to the primary sample of 36 high signal-to-noise ratio spectra whereas those in parentheses (and the shaded histograms) refer to the sample of 26 used to construct the mean UV spectra (see text).

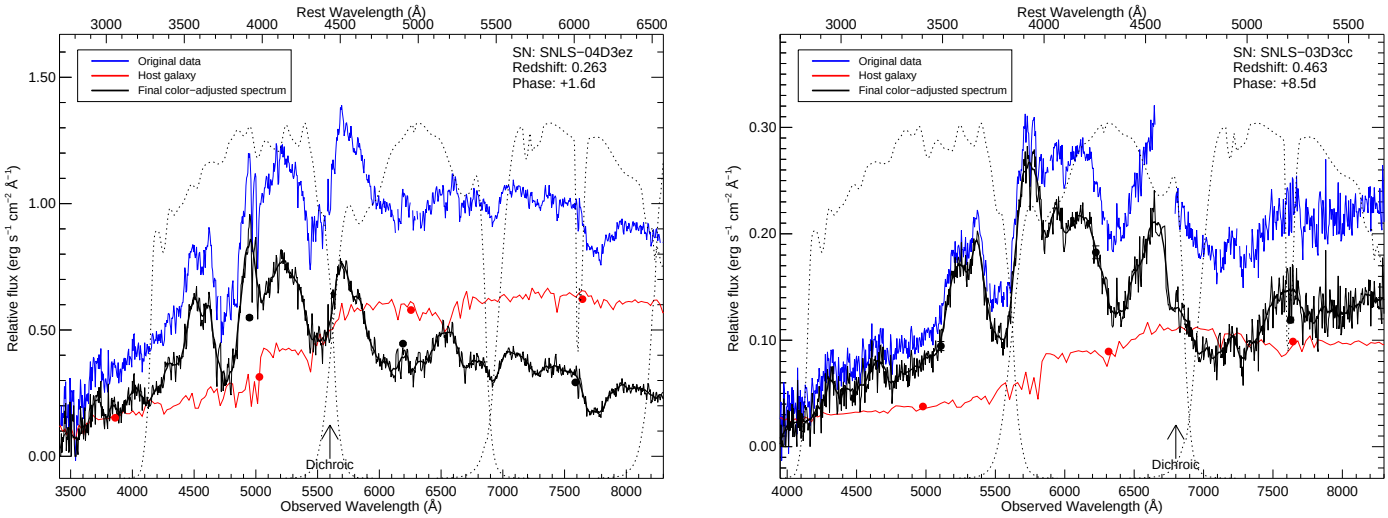

Fig. 2.— Examples of the host galaxy subtraction and flux calibration techniques for two SNe Ia suffering host contamination. The blue spectrum represents the observed data, the red spectrum the estimated host galaxy spectrum from fits to the broad-band galaxy $u^\star g'r'i'z'$ photometry (red circles), and the black spectrum is the host-galaxy subtracted final spectrum color-corrected to the $g'r'i'z'$ SN photometry (black circles). A smoothed version of the final spectrum is over-plotted, the heavy line denoting the spectral region deemed to have the most reliable flux calibration. The photometric points are plotted at the effective wavelengths of the filters on the appropriate spectrum, and the total system response through the $g'r'i'z'$ filters overplotted at the observed wavelengths. The position of the dichroic between the two arms of the spectrograph is also marked. Left (a): SNLS-04D3ez at $z = 0.263$. This SN had an increase in i' of $\sim 80\%$ on the day of observation. Right (b): SNLS-03D3cc at $z = 0.463$, with an increase in i' of $\sim 200\%$. Note that due to the color correction applied to the final spectrum, as plotted the black spectrum differs slightly from the simple subtraction of the red from the blue. [See the electronic edition of the journal for Figs. 2.3–2.26]

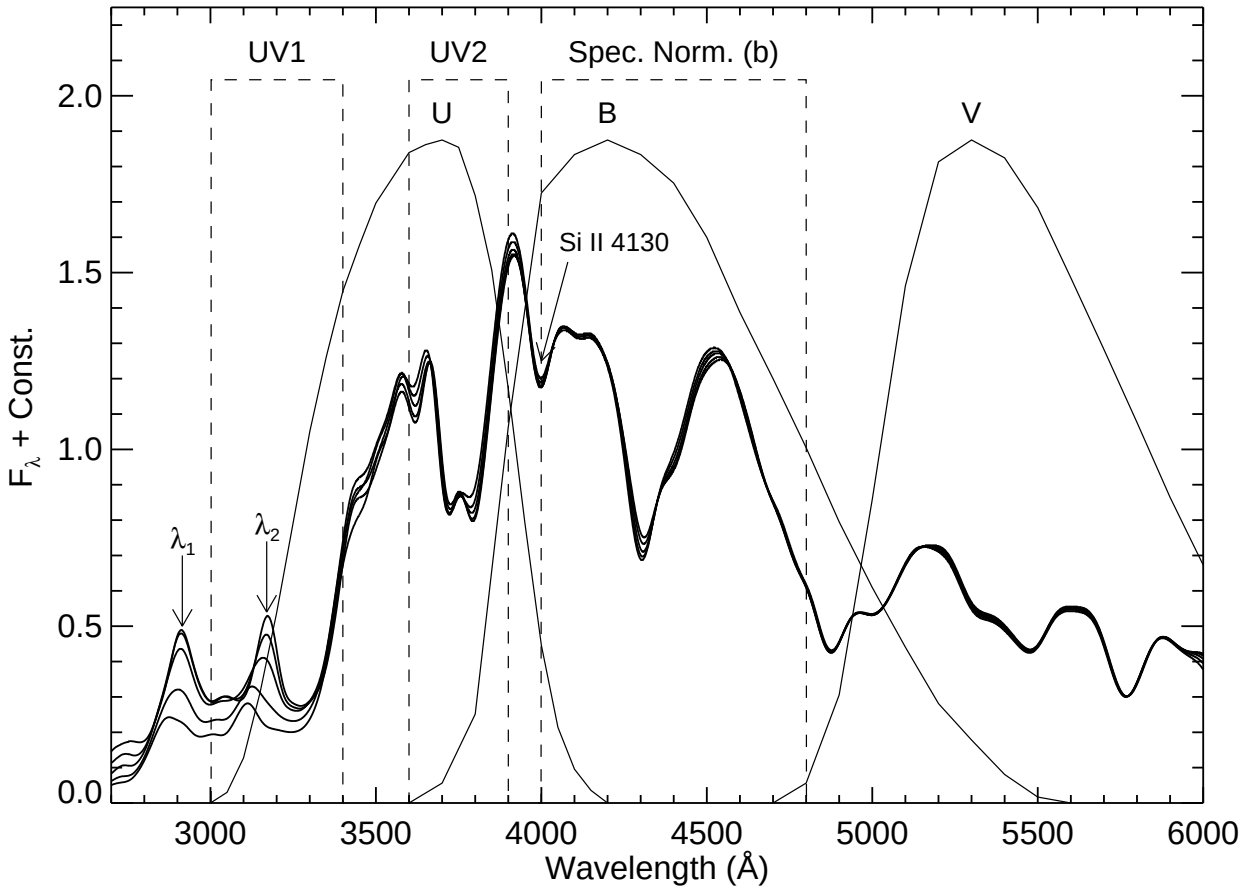

Fig. 3.— Maximum light SN Ia spectra from Lentz et al. (2000) at a variety of different metallicities (top to bottom: 0.1, 0.3, 1.0, 3.0 and 10.0 times solar metallicity). Over-plotted are the standard Bessell (1990) U and B filter responses, as well as the UV box filters ("UV1" and "UV2") and spectroscopic normalizing filter ("b") used in the analysis. Features thought to represent possible metallicity diagnostics (λ_1, λ_2) are also marked, as well as the position of the blue-shifted Si II 4130Å absorption feature.

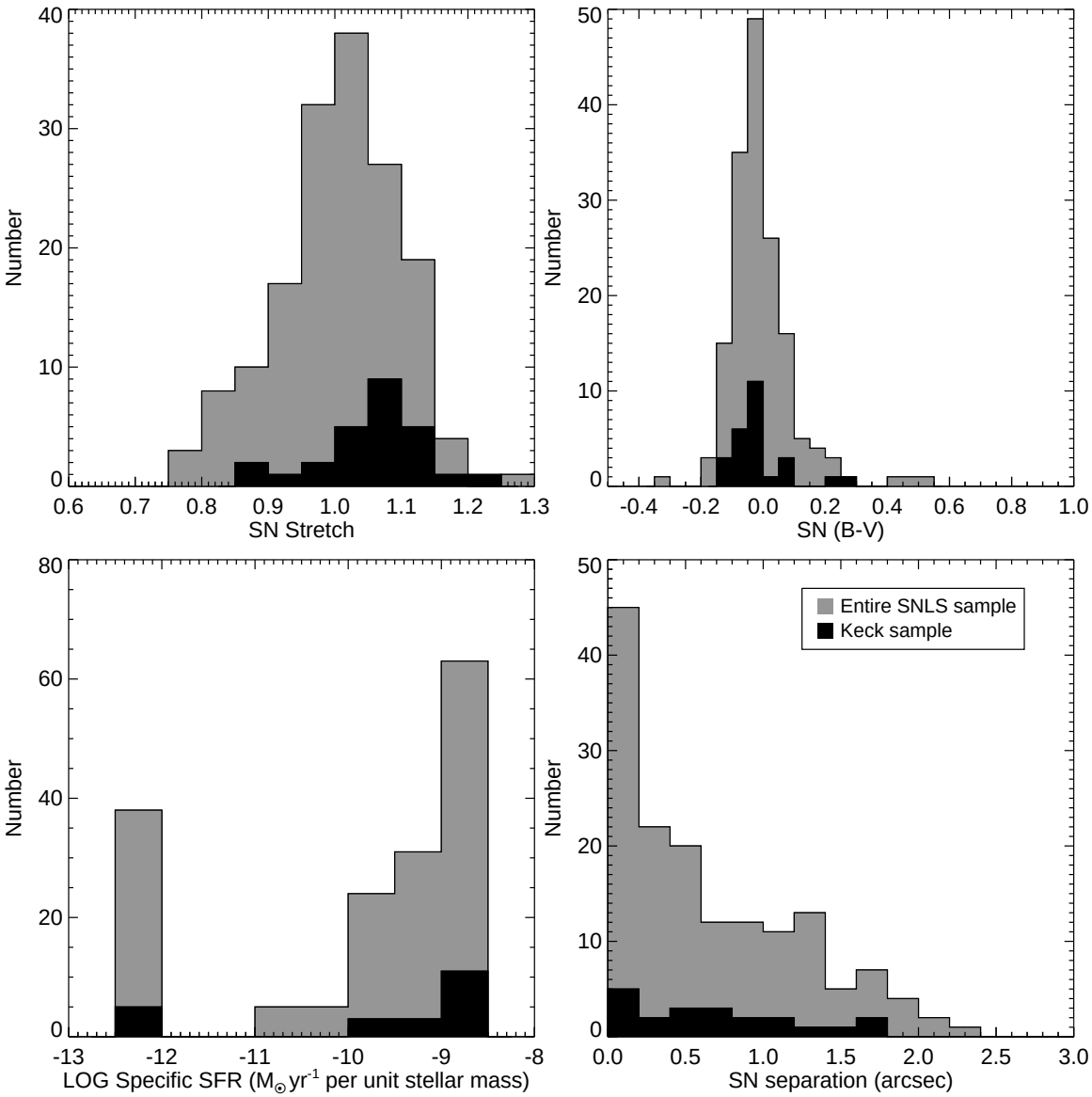

Fig. 4.— Comparison of SN stretch, SN B-V color, host galaxy specific star formation rate and SN/galaxy projected separation for the Keck SN Ia sample (black histogram; present paper) and the entire SNLS sample within the appropriate redshift range discovered over the same period (grey histogram). Galaxies with undetected star formation were placed at $10^{-12}\,M_{\odot}$ yr^{-1} per unit stellar mass.

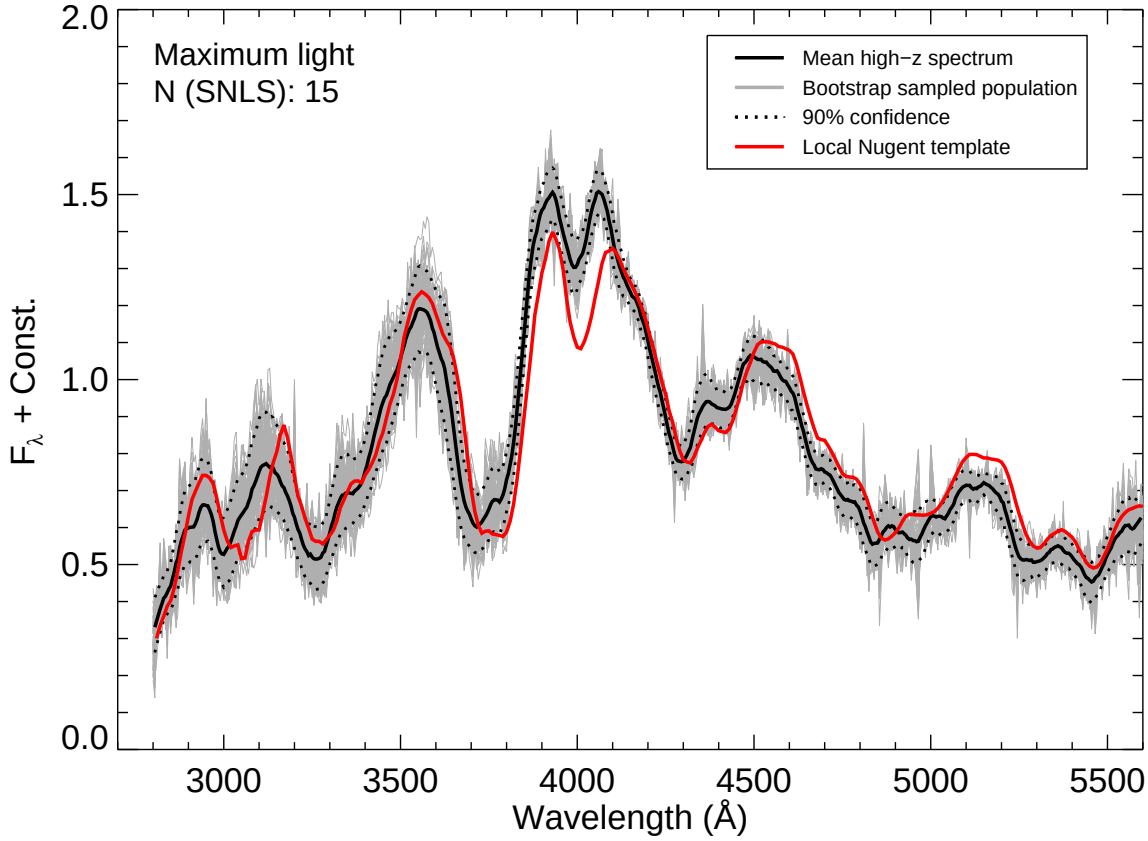

Fig. 5.— The mean high-redshift maximum light (effective day $< \pm$ 4 days) rest-frame UV SN Ia spectrum compared to the local average template of Nugent et al. (2002). Overplotted in light grey are 100 bootstrap-resampled mean spectra drawn from the high-redshift population; the dotted lines show the region containing 90% of this distribution. The local template has been color-adjusted to match the high redshift data.

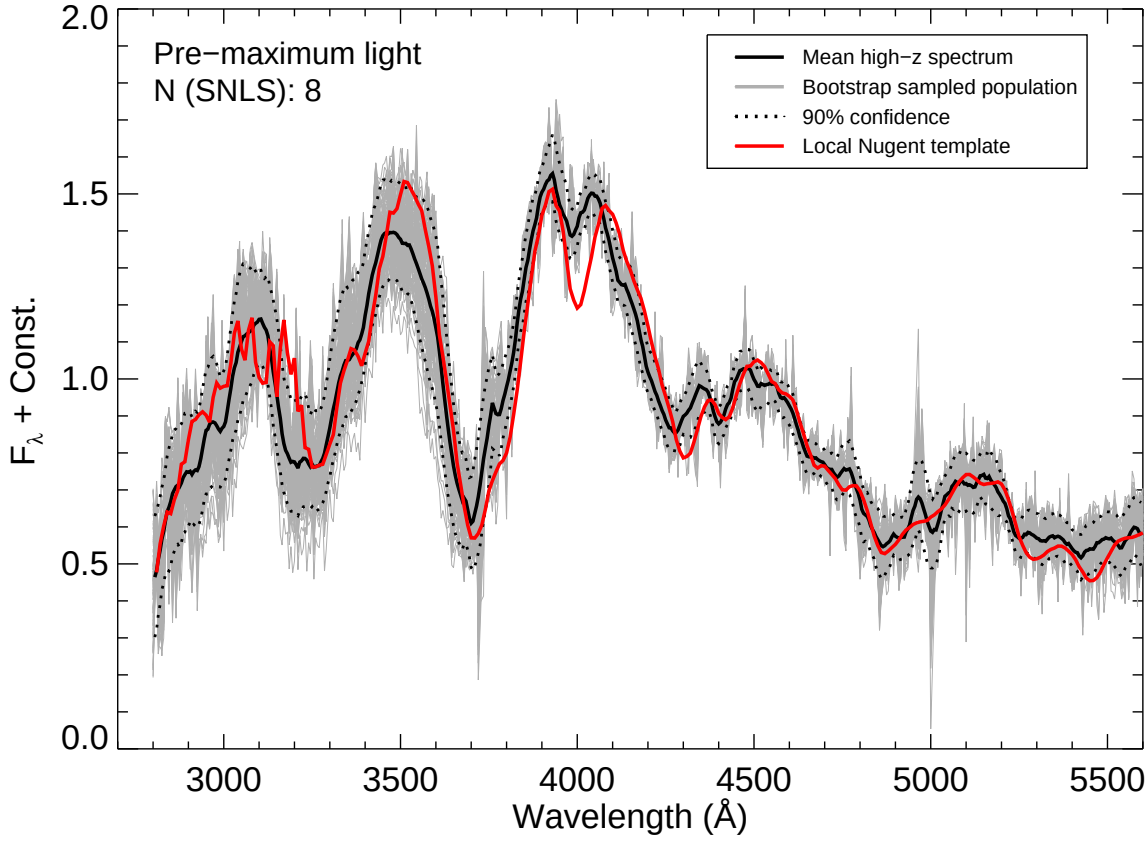

Fig. 6.— As Fig. 5, but showing the pre-maximum (effective day <-4 days) high-redshift spectrum versus the local template.

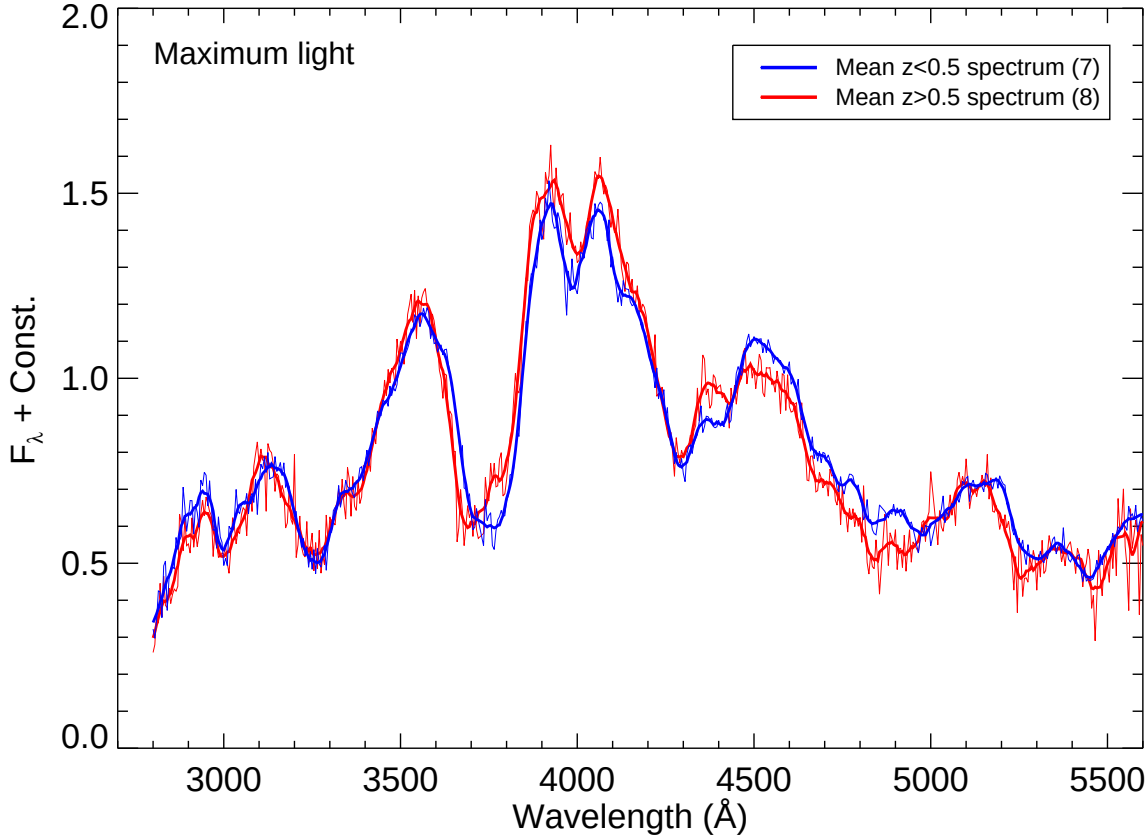

Fig. 7.— The mean high-redshift maximum light rest-frame UV SN spectrum split into two redshift intervals below (black) and above (red) z=0.5.

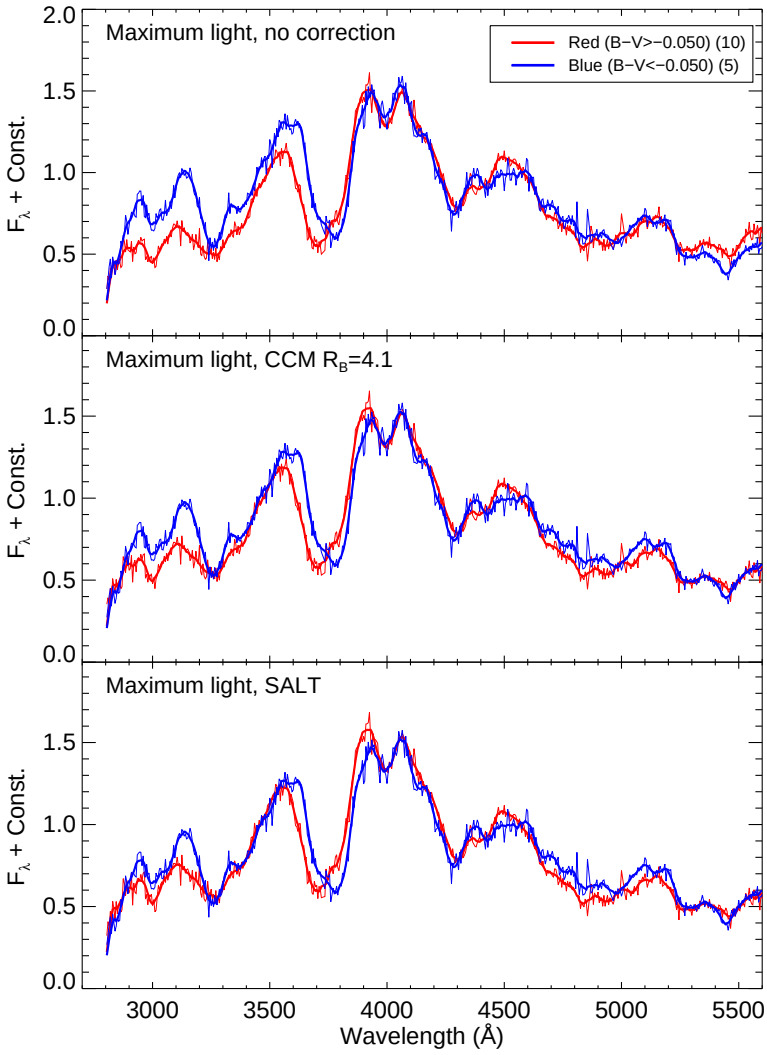

Fig. 8.— A test of the validity of applying a color correction to those Keck spectra sampled at maximum light. The top panel shows the mean *observed* spectrum for two subsamples split according to the rest-frame $B-V$ color at maximum light; red corresponds to SNe with $B-V > -0.057$, blue to those with $B-V <$-0.057. The middle panel shows the same comparison after applying a Cardelli et al. (1989) reddening correction to each individual spectrum using an $E(B-V)$ estimated from the light curve fits, and $R_B = 4.1$. Varying R_B has a negligible effect on this comparison. The lower panel shows the comparison after correcting individual spectra using the SALT color law (Guy et al. 2005).

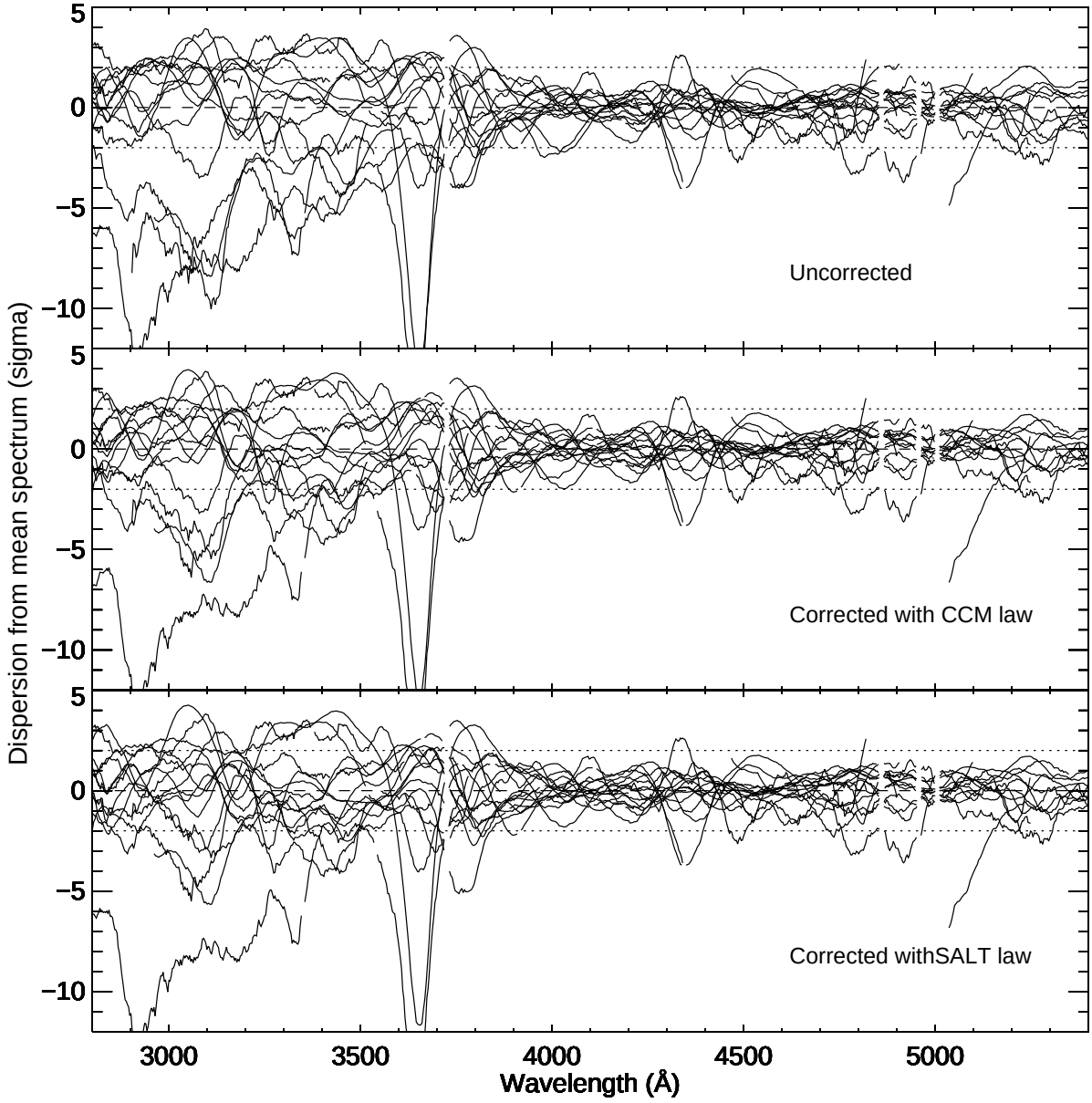

Fig. 9.— The deviation of the 15 maximum-light spectra from the mean spectrum in σ-units derived from their error spectra § 5.2.2. The top panel shows the uncorrected spectra, the middle panel the spectra corrected with the CCM dust law, and the lower panel spectra corrected with the SALT color law. The horizontal lines denote ± 2-σ deviations.

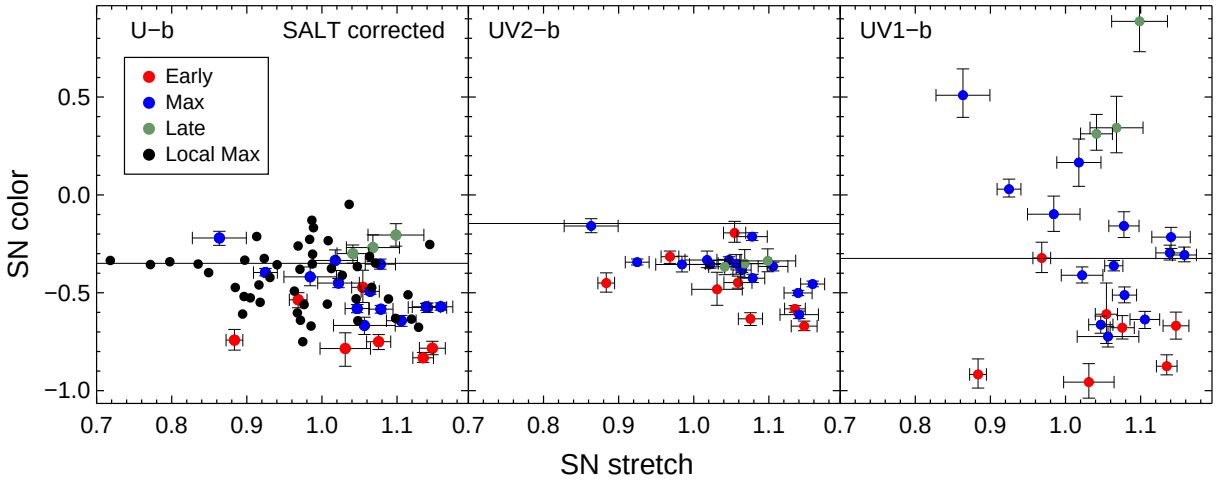

Fig. 10.— Various SN Ia stretch-color relations, with colors measured directly from the SALT color law corrected Keck spectra. The colors shown are $U-b$, $UV1-b$ and $UV2-b$ – see Fig. 3 for filter definitions. SNe are color-coded according to the phase of the spectrum as defined in Fig. 1. The black points in the $U-b$ distribution refers to the $U-b$ distribution of local SNe Ia at maximum light from local SN surveys (e.g. Jha et al. 2006). The error-bars for the SNLS SNe include propagated uncertainties from host galaxy subtraction (§ 3.3).

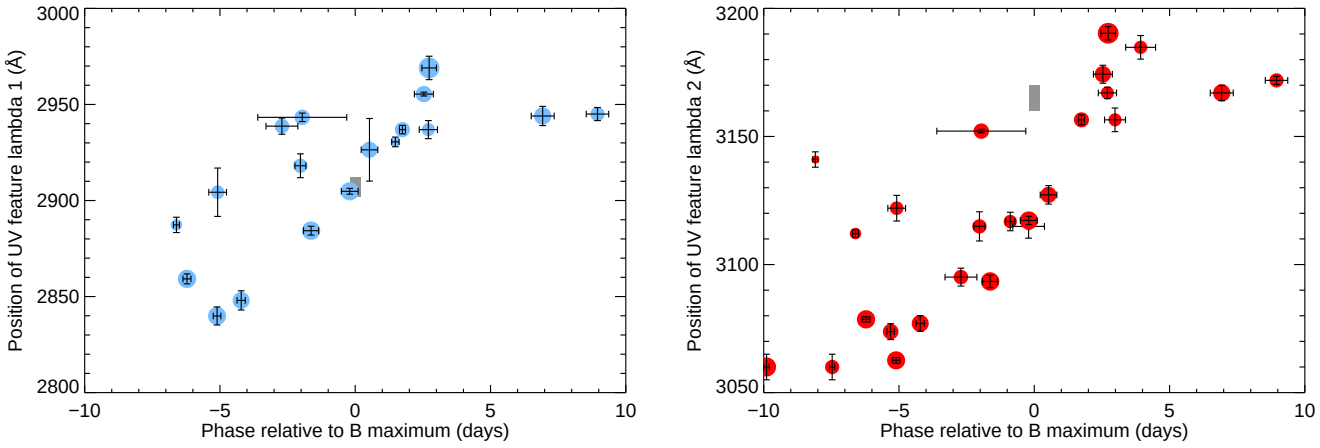

Fig. 11.— Variation of wavelength with phase for the two UV diagnostic features marked in Fig. 3; a clear trend is apparent. The vertical line refers to the full extent of the metallicity variation predicted by Lentz et al. (2000).

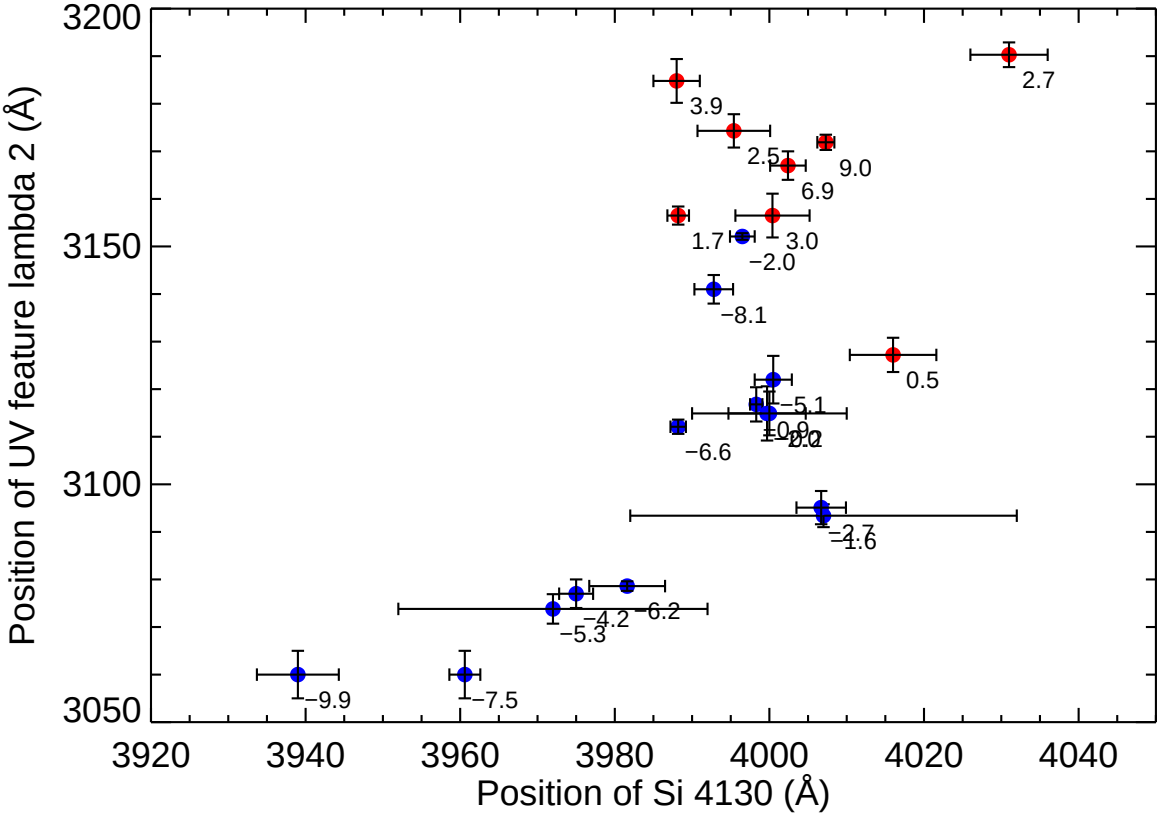

Fig. 12.— Comparison between the wavelength of the Si II 4130Å feature commonly used as a measure of the photospheric expansion velocity and that of the UV diagnostic λ_2 (see Fig. 3 for definition). Spectra taken before maximum light are indicated with blue symbols; those after maximum light with red symbols. Numbers indicate the phase in rest-frame days.

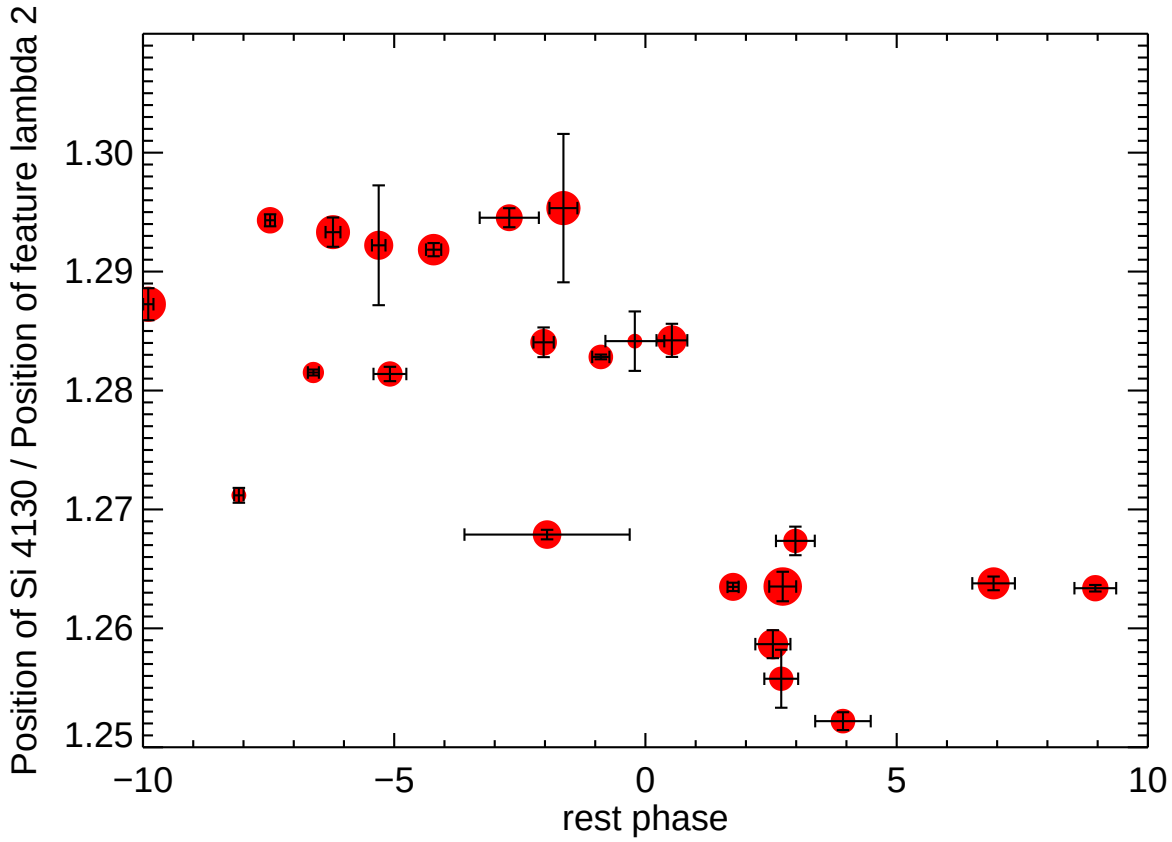

Fig. 13.— Ratio of the wavelength of the Si II 4130Å feature to the UV diagnostic λ_2 versus phase with data points sized according to the stretch. There is a clear discontinuity in the behavior after maximum light.

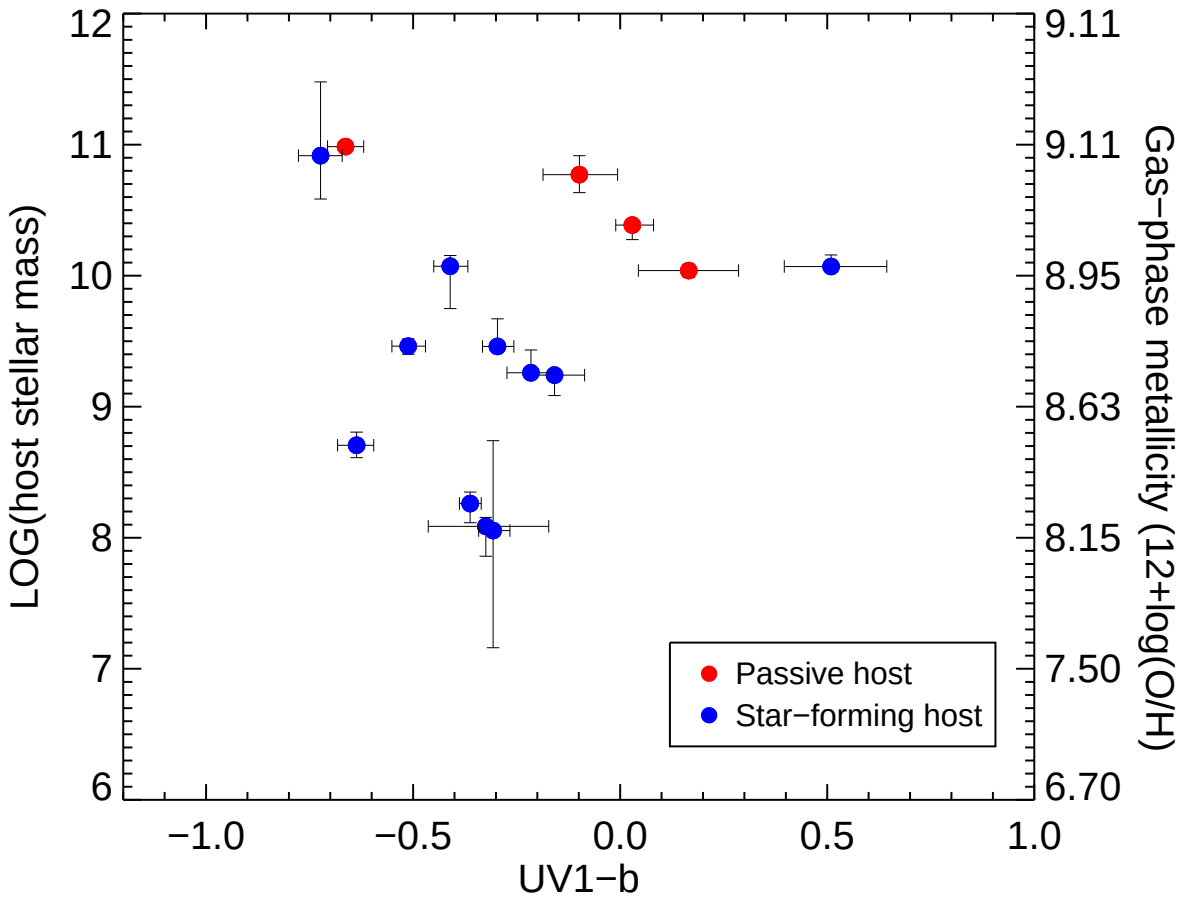

Fig. 14.— The variation of the Keck SN Ia $UV1 - b$ spectral color as a function of the stellar mass of the SN host galaxy color coded according to the specific star formation rate. The division is made at a rate of $10^{-12} M_{\odot}$ yr^{-1} per unit stellar mass. The color error-bars include propagated uncertainties from host galaxy subtraction. The conversion from stellar mass to gas-phase metallicity using the relation of Tremonti et al. (2004) is also shown.

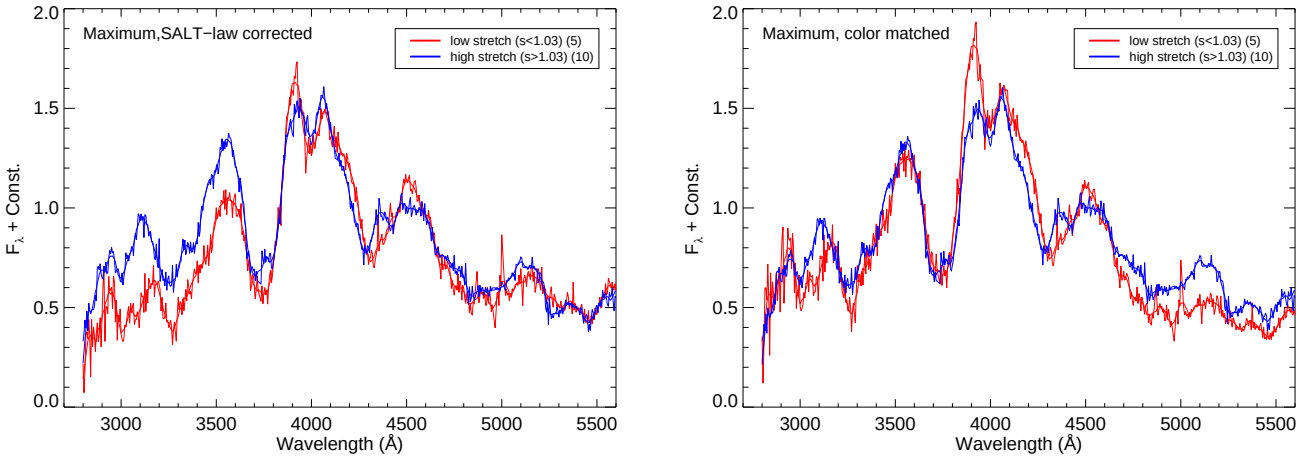

Fig. 15.— The mean SALT-law color-corrected (left) and color-matched (right) Keck spectra for SNe Ia split according to the SN light curve stretch, s. The red spectrum refers to events with $s \leq 1.03$, the blue spectrum to those with $s > 1.03$.

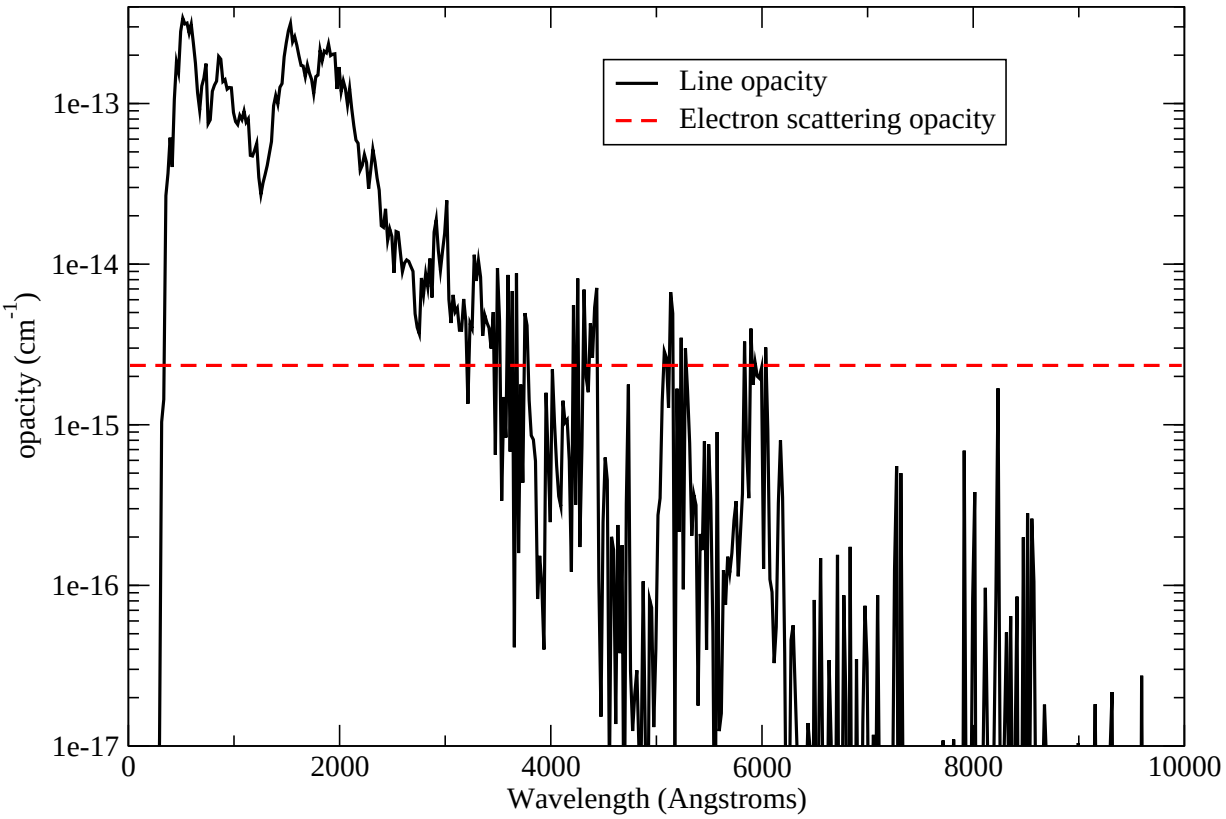

Fig. 16.— Comparison of the wavelength-dependent line and electron scattering opacity for a typical model in Kasen & Woosley (2007) at peak SN Ia brightness. The data refers to a depth of 7000 km s^{-1}. Note the drop in line opacity with respect to the electron scattering opacity near 4000 Å . This behavior makes the emergent UV flux highly sensitive to changes in the line opacity whereas the optical and near-IR spectral regions are largely dominated by electron scattering opacity.

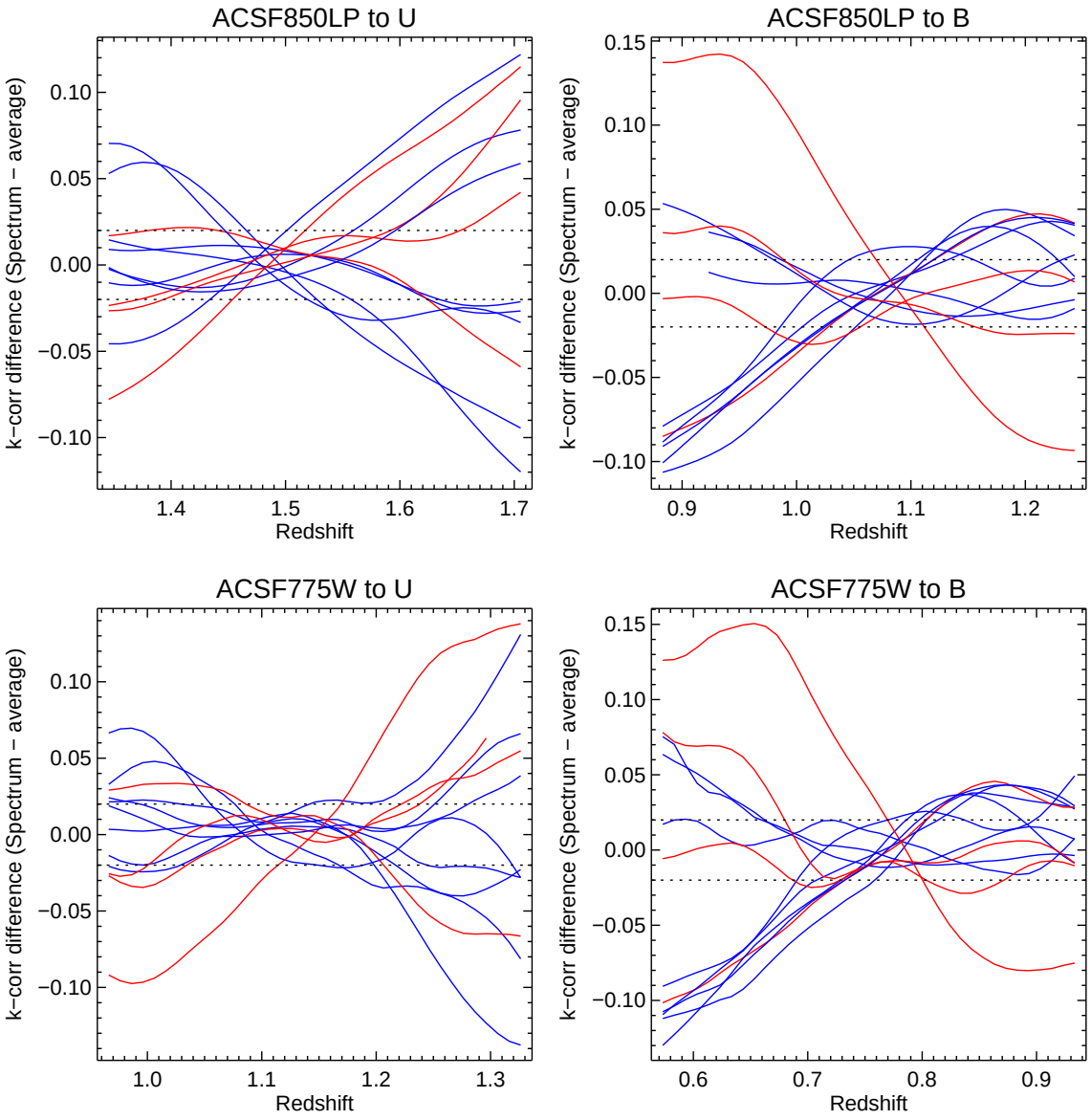

Fig. 17.— Redshift dependence of various maximum light cross-filter k-corrections differenced to that based on the local template. Lines represent deviations observed for individual Keck spectra color-coded according to stretch: red lines refer to events with $s \leq 1.03$, while blue to those with $s > 1.03$. The dashed lines indicates the approximate precision necessary to secure an equation of state parameter w to a precision of 5% using $z >$1 SNe Ia (see text for discussion).